Annals of Nuclear Energy 69 (2014) 74–89

Contents lists available at ScienceDirect

Annals of Nuclear Energy

journal homepage: www.elsevier.com/locate/anucene

Europium resonance parameters from neutron capture and transmission measurements in the energy range 0.01–200 eV

G. Leinweber [a,*], D.P. Barry [a], J.A. Burke [a], M.J. Rapp [a], R.C. Block [a], Y. Danon [b], J.A. Geuther [c], F.J. Saglime III [d]

[a] Bechtel Marine Propulsion Corp., Knolls Atomic Power Laboratory P.O. Box 1072, Schenectady, NY 12301-1072, United States
[b] Rensselaer Polytechnic Institute, Gaerttner LINAC Center, 110 8th St., Troy, NY 12180, United States
[c] Kansas State University, 3002 Rathbone Hall, Manhattan, KS 66506, United States
[d] Moog Inc., East Aurora, NY 14052, United States

ARTICLE INFO

Article history:
Received 6 December 2013
Accepted 31 January 2014

Keywords:
Europium
Transmission
Capture
Thermal cross section
RPI
Resonance parameters

ABSTRACT

Europium is a good absorber of neutrons suitable for use as a nuclear reactor control material. It is also a fission product in the low-yield tail at the high end of the fission fragment mass distribution. Measurements have been made of the stable isotopes with natural and enriched samples.

The linear electron accelerator center (LINAC) at the Rensselaer Polytechnic Institute (RPI) was used to explore neutron interactions with europium in the energy region from 0.01 to 200 eV. Neutron capture and transmission measurements were performed by the time-of-flight technique. Two transmission measurements were performed at flight paths of 15 and 25 m with ^{6}Li glass scintillation detectors. The neutron capture measurements were performed at a flight path of 25 m with a 16-segment sodium iodide multiplicity detector.

Resonance parameters were extracted from the data using the multilevel R-matrix Bayesian code SAMMY. A table of resonance parameters and their uncertainties is presented.

To prevent air oxidation metal samples were sealed in airtight aluminum cans in an inert environment. Metal samples of natural europium, 47.8 atom% ^{151}Eu, 52.2 atom% ^{153}Eu, as well as metal samples enriched to 98.77 atom% ^{153}Eu were measured.

The measured neutron capture resonance integral for ^{153}Eu is (9.9 ± 0.4)% larger than ENDF/B-VII.1. The capture resonance integral for ^{151}Eu is (7 ± 1)% larger than ENDF/B-VII.1.

Another significant finding from these measurements was a significant increase in thermal total cross section for ^{151}Eu, up (9 ± 3)% from ENDF/B-VII.1. The thermal total cross section for ^{153}Eu is down (8 ± 3)% from ENDF/B-VII.1, but it is larger than that of ENDF/B-VII.0.

The resolved resonance region has been extended from 100 eV to 200 eV for both naturally-occurring isotopes. Uncertainties in resonance parameters have been propagated from a number of experimental quantities using a Bayesian analysis. Uncertainties have also been estimated from fitting each Eu sample measurement individually.

1. Introduction

Europium is important in the design of light-water nuclear reactors for two reasons. First, europium is a fission product in the low-yield tail at the high end of the fission fragment mass distribution. Second, it is a strong neutron absorber that could be employed as a solid oxide control material. Europium is a slow-burning poison due to its 5-member chain of absorbing isotopes, mass numbers 151 through 155. Each of these isotopes has either high fission yield or high thermal neutron cross section.

The purpose of the present work was to determine resonance parameters for europium. The resonance parameters in ENDF/B-VII.1 (Chadwick et al., 2011) were adopted primarily from the measurement of Rahn et al., 1972). The Rahn et al. measurement utilized highly enriched oxide samples, consisted of transmission and self-indication experiments, and employed the synchrocyclotron at Columbia University. The current measurement has better energy resolution and updated analysis methods.

Other prominent experiments include Moxon et al. (1976) who measured capture cross sections averaged over 100 eV-wide

* Corresponding author. Tel.: +1 (518) 276 4006; fax: +1 (518) 2764007.
E-mail address: leinwg@rpi.edu (G. Leinweber).

http://dx.doi.org/10.1016/j.anucene.2014.01.041
0306-4549/

regions in 1976, Widder (1974) performed neutron capture measurements with a Moxon-Rae detector in 1974, Konks et al. (1968) used a lead slowing-down-time spectrometer to determine average capture cross sections in 1968, and Anufrijev et al. (1979) used a reactor in 1979. Recent experiments include Lee et al. (2010) in 2010 using a C_6D_6 capture detector at a 12 m flight path. Their results agreed with the JENDL-4.0 evaluation in the resolved resonance region. They used this agreement as validation of their weighting function. Parker et al. (2007) used the DANCE barium fluoride capture detector at the Los Alamos National Laboratory in 2007.

The release of the ENDF/B-VII.1 library in 2011 included an increase in the thermal total cross section of ^{153}Eu of 14% over the ENDF/B-VII.0 (Chadwick et al., 2006) value. The current measurement supports an increase by a smaller amount as discussed in Section 4.9.

2. Experimental conditions

2.1. Overview

Table 1 gives some details of the experimental conditions including neutron targets, overlap filters, LINAC pulse repetition rates, flight path lengths, and time-of-flight channel widths. The neutron energy for a detected event was determined using the time-of-flight (TOF) technique.

The nominal resolution, pulse width divided by flight path length, was ≈1 ns/m for epithermal transmission and capture measurements.

Thermal and epithermal capture and epithermal transmission were measured at a 25 m flight path. Thermal transmission was measured at 15 m. Thermal and epithermal transmission were measured with ^{6}Li glass detectors (Barry, 2003; Leinweber et al., 2002; Leinweber et al., 2010; Trbovich, 2003). Thermal and epithermal capture were measured with a 16-segment NaI detector (Barry, 2003; Leinweber et al., 2002; Leinweber et al., 2010; Trbovich, 2003), (Block et al., 1988).

The LINAC was used to accelerate electrons into a tantalum target. Bremsstrahlung radiation and photoneutrons were produced. The neutron-producing targets were optimized for each energy range (Danon et al., 1993; Danon et al., 1995; Overberg et al., 1999).

Table 2 gives some sample information including the sample thickness, atom fraction of each isotope, and measurements.

The uncertainties in sample thickness were propagated from multiple measurements of sample weight and diameter. The diameter measurements were the dominant component of the uncertainties. All samples were mounted in aluminum sample cans. The thickness of aluminum on each of the front and rear faces of each sample was 0.38 mm. The influence of these sample cans, as well as all background, was measured by including empty sample cans in all measurements. Background in transmission measurements is discussed in Section 3.2.1.

2.2. Sample Information

There are only two naturally-occurring isotopes of europium (see Table 2). The samples measured were elemental as well as enriched to 98.77 atom% ^{153}Eu. Europium is a highly-reactive metal, and care was taken to prevent oxidation. Metallic samples for both natural and enriched Eu were fabricated, weighed, and encapsulated in an inert atmosphere. X-ray imaging of the encapsulated thin metal disks was performed, and the images were analyzed to identify any non-uniformity of thickness (Geuther et al., 2013).

X-ray images of the samples used in these experiments are shown in Fig. 1. A samarium step-wedge was used to calibrate X-ray image data and quantify the non-uniformity of sample thickness. Samarium was chosen as the step-wedge material because it has nearly the same mass attenuation coefficient as europium. Additionally, samarium is much less reactive in air and could be imaged next to the encapsulated (in 0.38 mm Al) Eu samples. Fig. 1 is reprinted from Ref. (Geuther et al., 2013). The sample thicknesses are given in Table 2. They were determined from measurements of mass and area made at the time of encapsulation, not from the subsequent X-ray images. The X-ray imaging results for average sample thickness provided confirmation of both the thicknesses and the methods. The relative density profiles from the imaging measurements were included in the SAMMY analysis. There were no visible signs of oxidation at the time of encapsulation, which was done in an inert environment. The ^{153}Eu-enriched samples were provided by the Oak Ridge National Laboratory. The natural samples were obtained from the KAMIS Corporation. All samples were certified >99.9 weight percent europium. The results of mass spectrographs performed on the europium samples by their vendors are given in Table 3.

2.3. Capture detector

The capture detector is a gamma detector containing 20 l of NaI(Tl) divided into 16 optically-isolated segments (Block et al., 1988). The scintillation crystals form an annulus around the neutron beam with the sample at its center. The neutron beam was

Table 1
Europium experimental details.

Experiment	Overlap filter	Neutron-producing target	Elec-tron pulse width (ns)	Ave. beam current (μA)	Beam energy (MeV)	Energy region (eV)	Channel width, (μs)	Pulse repetition rate (pulses/s)	Flight path length (m)
Epithermal transmission	Boron carbide	Bare bounce	25	11	58	$E < 15$ $15 < E < 800$ $E > 800$	0.4096 0.1024 0.0256	225	25.590 ± 0.006
Thermal transmission	None	Enhanced thermal target	540	8	55	$E < 0.05$ $0.05 < E < 1.4$ $1.4 < E < 5.6$ $E > 5.6$	26.214 3.2768 0.8192 0.4096	25	14.96 ± 0.02
Epithermal capture	Cadmium	Bare bounce	19	13	56	$E < 15$ $15 < E < 800$ $E > 800$	0.4096 0.1024 0.0256	305	25.564 ± 0.006
Thermal capture	None	Enhanced thermal target	560	8	56	$E < 0.05$ $0.05 < E < 1.4$ $1.4 < E < 5.6$ $E > 5.6$	26.214 3.2768 0.8192 0.4096	25	25.446 ± 0.002

Table 2
Sample details.

Nominal thickness	Areal density (atoms/barn)	Uncertainty (atoms/barn)	Atom fraction	Measurements
0.127 mm (0.005 in)	2.6E-04	3E-05	^{151}Eu: 0.478 ^{153}Eu: 0.522	Thermal capture and transmission
0.254 mm (0.010 in)	4.5E-04	1E-05	^{151}Eu: 0.478 ^{153}Eu: 0.522	Thermal transmission, epithermal capture
0.508 mm (0.020 in)	1.027E-3	3E-06	^{151}Eu: 0.478 ^{153}Eu: 0.522	Thermal and epithermal capture
1.016 mm (0.040 in)	2.105E-3	3E-6	^{151}Eu: 0.478 ^{153}Eu: 0.522	Epithermal transmission
0.127 mm (0.005 in)	2.4E-04	1E-05	^{151}Eu: 0.0123 ^{153}Eu: 0.9877	Thermal capture and transmission, epithermal capture
0.254 mm (0.010 in)	4.7E-04	2E-05	^{151}Eu: 0.0123 ^{153}Eu: 0.9877	Thermal and epithermal capture
0.381 mm (0.015 in)	7.2E-04	2E-05	^{151}Eu: 0.0123 ^{153}Eu: 0.9877	Thermal capture and transmission, epithermal transmission

Note: The precision of the values in Table 2 reflect differences between the vendors of the natural and enriched samples.

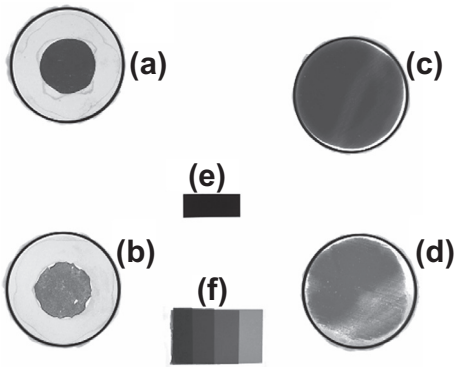

(a) 10-mil Eu-153 sample
(b) 5-mil Eu-153 sample
(c) 10-mil elemental Eu sample
(d) 5-mil elemental Eu sample
(e) 1 in.x 1 cm. gauge
(f) Sm step wedge

Fig. 1. X-ray image of Sm step wedge, measurement gauge, and several elemental and isotopic Eu samples taken at St. Peter's Hospital in Albany, NY on October 1, 2009, with a 64.5 kVp, 40 mAs X-ray exposure. One mil = 0.001 in. = 0.00254 cm. This figure is reprinted from Ref. (Geuther and J.A., 2013). The apparent holes in sample (b) were accounted for in the resonance parameter analysis.

collimated to a diameter of 2.54 cm at the sample position. Neutrons that scatter from the sample are absorbed by a 0.9-cm-thick hollow cylindrical liner fabricated of 98.4 w/o ^{10}B carbide ceramic to reduce the number of scattered neutrons reaching the gamma detector. The discriminator on each detector section was set to 100 keV. A total energy deposition of 1 MeV for the epithermal measurement and 2 MeV for the thermal measurement was required to register a capture event. Therefore, the system discriminates against the 478 keV gamma rays from $^{10}B(n;\alpha,\gamma)$ absorptions.

The efficiency of the capture detector is about 75% for a single 2 MeV gamma ray. The efficiency of detecting a capture event in europium is close to 100% since, on average, 3–4 gamma rays are emitted for each capture event. Capture in ^{151}Eu leading to the isomer ^{152m}Eu was estimated to reduce detector efficiency by 0.05% and was neglected.

The samples were precisely positioned at the center of the detector by a computer-controlled sample changer. The dead time of the system was 1.125 μs, and the dead time correction factor was less than 3% for the thermal measurement and under 1% for epithermal.

2.4. Transmission detectors

The epithermal neutron transmission measurement was conducted at the 25-meter flight station. It utilized a 12.70-cm (5-in) diameter, 1.27-cm-thick ^{6}Li glass scintillator housed in a light-tight aluminum box and viewed by two photomultiplier tubes that are out of the neutron beam. The details of this detector design are given in Ref. (Barry, 2003). The measurement with this detector covered the range of incident neutron energies from 10 eV to 200 eV.

Table 3
Impurities in the europium samples.

Impurity	Natural samples (ppm)	^{153}Eu-enriched samples (ppm)
Fe	81	<100
Ca	60	N/A
Cl	44	N/A
S	32	N/A
Si	26	<100
K	20	N/A
Al	17	<100
Mg	N/A	<100
Ni	N/A	<100
Y	N/A	<100
Gd	N/A	<100
Nd	N/A	<100
Sm	N/A	<100
Tb	N/A	<100
All Others	<10	N/A

The thermal transmission measurement was conducted at the 15-m flight station. The 15-m flight station contains a 7.62-cm (3-in) diameter, 0.3-cm-thick NE 905 ^{6}Li glass scintillation detector (6.6% lithium, enriched to 95% in ^{6}Li) and was used for measurements covering the energy range from 0.01 eV to 30 eV. The detector is coupled to a single photomultiplier tube.

Transmission samples along with empty sample holders, which are used to measure the open-beam count rate, were mounted on an 8-position computer-controlled sample changer. The transmission can be expressed as a function that is approximately the ratio of the count rate with a sample in the beam to the count rate with samples removed. The transmission can vary strongly with incident neutron energy and is directly linked to the total cross section of the sample material being measured. Each data run consisted of one complete cycle through the samples, with a predetermined number of LINAC pulses for each sample position. The distribution of pulses per sample position was chosen to minimize the counting statistical error in the measured cross section (Danon and Block, 2002). The dead time correction factor was less than 1%.

3. Data reduction

3.1. Capture data

Processed capture data are expressed as yield. Yield is defined as the number of neutron captures per neutron incident on the sample. The capture yield, Y_i, in time-of-flight channel i, was calculated by:

$$Y_i = \frac{C_i - B_i}{K(\phi_i - B_{\phi_i})} \quad (1)$$

where C_i is the dead-time-corrected and monitor-normalized counting rate of the sample measurement, B_i is the dead-time-corrected and monitor-normalized background counting rate, K is the product of the flux normalization factor and efficiency, and φ_i is the measured neutron flux shape. B_{ϕ_i} is the dead-time-corrected and monitor-normalized background counting rate in the measured flux shape.

In addition to the sample data, another set of data was needed to determine the energy profile of the neutron flux. This was done by mounting a 2.54-mm thick, 98.4% enriched $^{10}B_4C$ sample in the sample changer and adjusting the total energy threshold to record the 478 keV gamma rays from neutron absorption in ^{10}B. These flux data were corrected for transmission through the boron sample. The thermal flux was smoothed using 101-point adjacent averaging. The epithermal flux contained the complex structure of the cadmium filter and was not smoothed. The resulting resonance parameters from the epithermal data had a larger uncertainty without the smoothing. The magnitude of the flux was normalized to a black capture resonance, the 3.368 eV resonance in ^{151}Eu for the epithermal measurement, and the 0.46 eV resonance in ^{153}Eu for the thermal measurement. The two isotopes are both odd-A and have similar neutron binding energies. So, their gamma cascades are expected to be similar, and thus their gamma detection efficiencies are also similar.

The zero time-of-flight was obtained from the measured location of the gamma flash resulting from the electron pulse.

The background in capture was determined from in-beam measurements of empty sample holders. The capture yield and its associated statistical uncertainty provided input to the SAMMY (Larson, 2008) data analysis code that extracted the neutron resonance parameters. Systematic components of resonance parameter uncertainties are discussed in Section 4.9.

The signal-to-background ratios for the Eu capture and transmission measurements are shown in Fig. 2. The value from thermal capture reached a peak of ≈130 at 0.08 eV, then remained >50 up to 30 eV.

The signal-to-background ratio in the epithermal capture experiment was ≈3 at 10 eV and increased almost linearly to ≈16 at 200 eV. The flux-to-background ratio was smaller than recent measurements at the RPI LINAC (Barry, 2003; Leinweber et al., 2002; Leinweber et al., 2010; Trbovich, 2003) because the neutron beam was collimated to a diameter smaller than 2.54 cm to accommodate the enriched ^{153}Eu samples (see Fig. 1). The typical beam diameter at the RPI LINAC has been 5.08 cm.

Further discussion of neutron capture data taking and data reduction techniques at the RPI LINAC were described in Ref. (Leinweber et al., 2002).

3.2. Transmission data

The transmission is given by Eq. (2).

$$T_i = \frac{(C_i^S - K_S B_i - B_S)}{(C_i^O - K_O B_i - B_O)} \quad (2)$$

where T_i, the transmission in time-of-flight channel i, C_i^S and C_i^O are the dead-time corrected and monitor-normalized counting rates of the sample and open measurements in channel i, respectively, B_i is the unnormalized, time-dependent background counting rate in channel i, B_S and B_O are the steady state background counting rates for sample and open measurements, respectively, and K_S and K_O are the normalization factors for the sample and open background measurements.

The signal-to-background ratio for the transmission measurements are shown in Fig. 2. The value for the epithermal measurement was 26 at 10 eV, then rose steadily to a peak of 85 at 100 eV, then reduced slowly to 80 at 200 eV. The signal-to-background ratio for the thermal transmission measurement was 260 at 0.01 eV, then rose steadily to a peak >2500 at 0.06 eV, then reduced quickly to ≈500 at 0.2 eV, then reduced gradually to ≈50 at 10 eV and ≈20 at 30 eV.

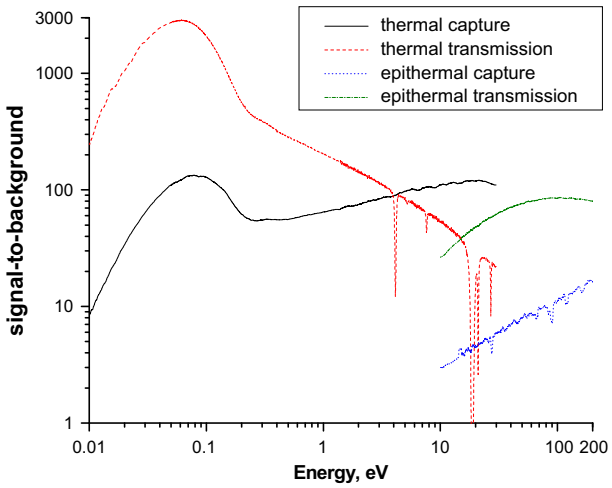

Fig. 2. The signal-to-background ratio for the Eu measurements.

3.2.1. Transmission background

Transmission background is a crucial aspect of a total cross section measurement. Transmission background was determined with a fixed notch filter and a dedicated set of measurements employing notch filters. A notch filter is an element with a strong, saturating (or black) resonance at an energy of interest. Any counts observed under a black resonance are attributed to background.

The fixed notch filter for the epithermal measurement was sodium at 2850 eV. A separate measurement was performed using a suite of materials with saturating resonances including silver at 5.2 eV, tungsten at 18.8 eV, cobalt at 132 eV, manganese at 336, 1100, and 2370 eV, and sodium at 2850 eV. Single- and double-thicknesses of these notch filters were placed in the beam and measured with each Eu sample. The one-notch and two-notch data were used to extrapolate to zero-notch thickness. The resulting background shape was normalized to the fixed notch at 2850 eV.

Thermal transmission time-dependent background was determined from a suite of notch filters including tungsten at 18.8 eV, silver at 5.2 eV, indium at 1.46 eV, and Cd at 0.178 eV. The thermal background shape was normalized to a fixed notch of tungsten at 18.8 eV.

4. Results

4.1. Resonance parameters

Thermal and epithermal neutron capture and transmission experiments were performed to resolve europium resonances between 0.01 and 200 eV. An overview of the data, the R-matrix Bayesian resonance parameter fit, and ENDF/B-VII.1 is shown in Figs. 3–6. Overall, seven samples were measured in transmission and capture. Sample details are given in Table 2.

Resonance parameters neutron width, Γ_n, radiation width, Γ_γ, and resonance energy, E were extracted from the capture and transmission data sets using the multi-level R-matrix Bayesian code SAMMY version 8 (Larson, 2008). Both capture and transmission data have been fitted to a single set of resonance parameters in the region below 200 eV. This was a combined transmission and capture analysis, which employed the experimental resolution, Doppler broadening, self-shielding, and multiple-scattering

features of SAMMY. The resulting resonance parameters of europium are listed in Table 4. In the table, resonance parameters and their uncertainties are given and compared to ENDF/B-VII.1. The first four columns are resonance energy and uncertainties, the next four columns are radiation width and uncertainties, then four columns of neutron width information, followed by isotope and spin (J). The measured value, the Bayesian and external uncertainties, and the ENDF/B-VII.1 values are given in Table 4 for each of the resonance parameters, resonance energy, neutron width, Γ_n, and radiation width, Γ_γ. Because europium lies near the peak of the s-wave strength function and near the minimum of the p-wave strength function all of the resonances in ^{151}Eu and ^{153}Eu below 200 eV were treated as s-wave, i.e., angular momentum, $\ell = 0$. The Bayesian uncertainty for each resonance in Table 4 was propagated from the multi-sample SAMMY fit of transmission and capture data. Internal and external uncertainties are defined and described in Section 4.10.8. The sample-to-sample external uncertainties given in brackets in Table 4 for each resonance are an estimate of the consistency within the current data. This external uncertainty is usually larger than the Bayesian error when there are many samples, but above 30 eV the SAMMY uncertainty estimates are usually larger. The number of significant figures displayed for the central value of the resonance parameters in Table 4 reflects the larger of the two uncertainties.

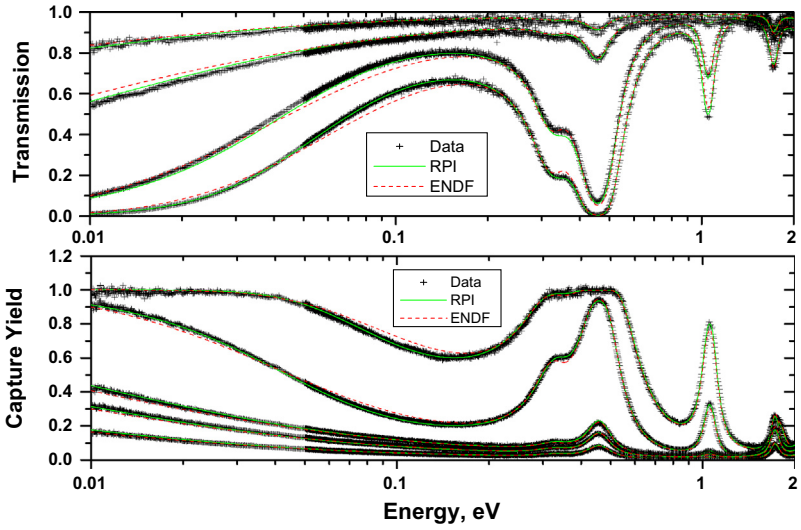

Fig. 3. Overview of the thermal Eu data and the resonance parameter fits. The lower two data sets of the upper plot and the upper two data sets of the lower plot are natural Eu data. The other five data sets are ^{153}Eu-enriched data. The natural Eu data are distinctive in that they include all of the resonances of ^{151}Eu and ^{153}Eu, and they display much larger thermal cross sections because they include ^{151}Eu. A single set of resonance parameters were fitted and used for the curve labeled 'RPI". Resonance parameters of negative energy resonances were changed to fit the shape of the data in the thermal region.

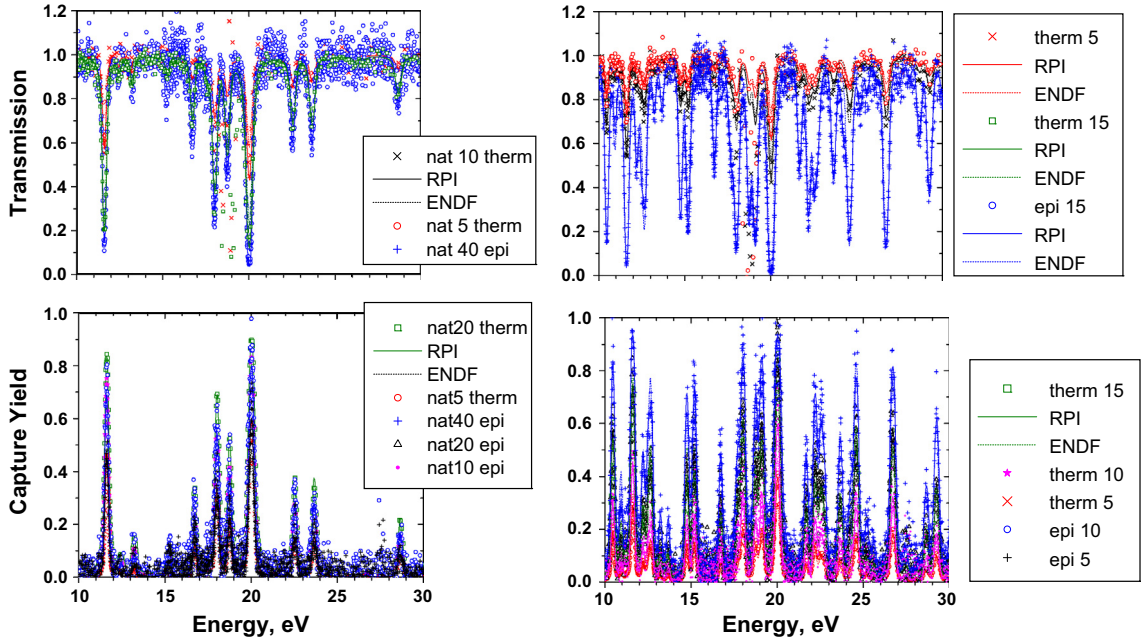

Fig. 4. The two plots on the left are from the natural Eu samples. The two plots on the right are from the ^{153}Eu-enriched samples. The top plots are transmission. The bottom plots are neutron capture. All samples, all measurements were used in the 10–30 eV region. The thermal data has excellent signal-to-background; the epithermal data have excellent energy resolution. Both data sets were used in the analysis of resonance parameters in the 10–30 eV energy region. Natural Eu samples and those enriched to 98.77% ^{153}Eu were measured and analyzed. The natural Eu samples were 47.8% ^{151}Eu, 52.2% ^{153}Eu. Curve labels specify energy region (thermal or epithermal) and sample thickness (5, 10, 15, 20, or 40-mils), where one mil = 0.001 in. = 0.000254 cm. The scatter in the transmission data near 18 and 27 eV is due to fixed neutron beam filters.

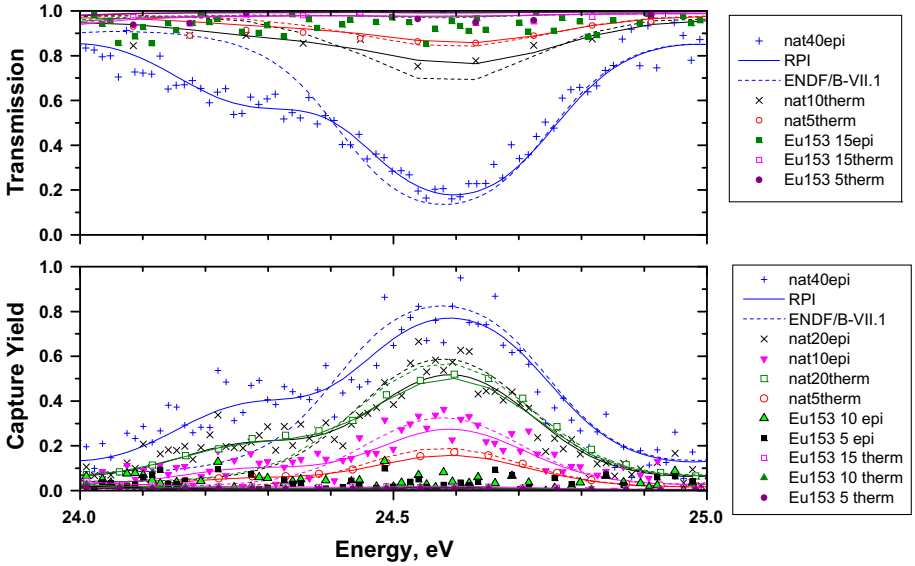

Fig. 5. A strong resonance in ^{151}Eu at ≈24.6 eV is prominent in the natural Eu sample data. The dashed lines, corresponding to the ENDF/B-VII.1 library, do not show the accompanying ^{151}Eu resonance at ≈24.3 eV. This "NEW" resonance is recommended by the present measurement. Data from the ^{153}Eu-enriched samples show neither resonance. The solid lines for all samples are the RPI parameters. The dashed lines for all samples are ENDF/B-VII.1. Curve labels specify isotopic content (natural or ^{153}Eu-enriched), energy region (thermal or epithermal) and sample thickness (5, 10, 15, 20, or 40-mils), where one mil = 0.001 in. = 0.000254 cm.

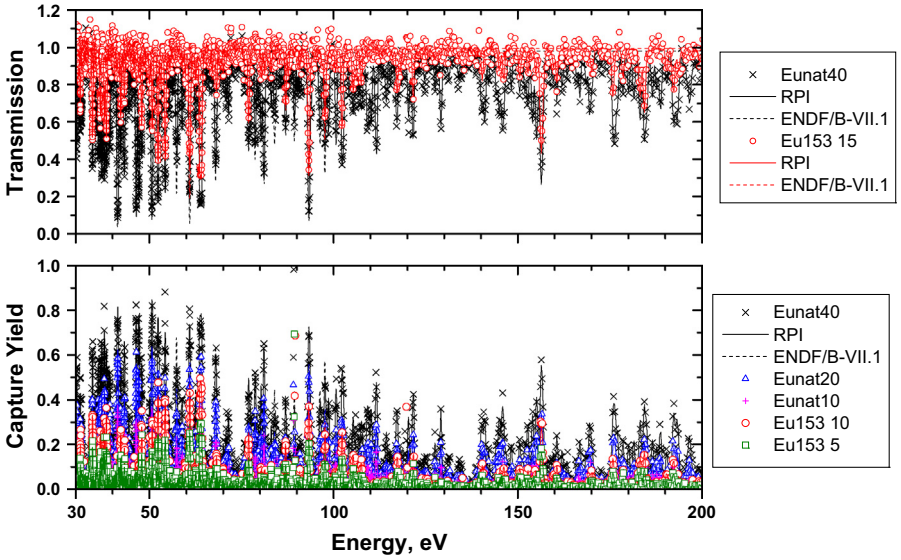

Fig. 6. Experimental results in the epithermal region above 30 eV. Transmission and capture data from natural Eu and enriched ^{153}Eu samples were acquired and analyzed. The solid lines for all samples are the RPI parameters. The dashed lines for all samples are ENDF/B-VII.1. Curve labels specify isotopic content (natural or ^{153}Eu-enriched), energy region (thermal or epithermal) and sample thickness (5, 10, 15, 20, or 40-mils), where one mil = 0.001 in. = 0.000254 cm. The ENDF curves appear as horizontal lines at $T \approx 0.98$ for $E > 100$ eV. The ENDF resolved resonance region ends at 100 eV for ^{151}Eu and ^{153}Eu. The cadmium filter in the capture measurement led to divergent transmission points near the strong Cd resonance at 90 eV.

Better fits using the new resonance parameters were evident throughout the energy spectrum. New resonances have been added at 12.524, 24.266, 47.42, 57.18, 65.49, 78.83, 84.19, 93.97, 95.93, 96.54, 98.02 eV, and beyond the end of the ENDF resolved resonance region above 100 eV. Below 100 eV the angular momentum states were assigned arbitrarily. Above 100 eV the spin was left unassigned, and the values in the columns labeled Γ_n and $\Delta\Gamma_n$ are values of 2 gΓ_n. An example of a new resonance within the current ENDF resolved resonance region is shown in Fig. 5. In the energy region 24–25 eV shown in the figure only two resonances are present; both are in ^{151}Eu. There is no structure in any of the ^{153}Eu-enriched sample data. In the region between 10 and 30 eV all data, natural and ^{153}Eu-enriched, transmission and capture, and thermal and epithermal were included in the fit. Above 30 eV thermal data were not included in the fits due to their poor energy resolution and lack of background information. Below 10 eV the signal-to-background ratios of the epithermal data were significantly poorer than those from the thermal measurements. The specific values are given in Section 3.1.

The resolved resonance region in ENDF, JEFF, and JENDL ends at 100 eV for ^{151}Eu and ^{153}Eu. This measurement provides resonance parameters up to 200 eV. Examples of the newly defined resonances are shown in Fig. 7. The figure gives an example of the current resonance treatment in the 140–160 eV region. There are no resonance parameters from ENDF in this energy region. Table 4 gives resonance parameters that extend the resonance region up to 200 eV.

Table 4
Resonance parameters for europium compared with ENDF/B-VII.1 parameters. Two uncertainties are given for each parameter, the Bayesian uncertainty from the SAMMY fit and an external error, in brackets, which conveys the agreement among individual sample fits as described in Section 4.10.

E,eV	ΔE Bayesian	[external]	Eendf	$\Gamma\gamma$	$\Delta\Gamma_\gamma$ Bayesian	[external]	$\Gamma_\gamma$endf	Γ_n	$\Delta\Gamma_n$ Bayesian	[external]	$\Gamma_n$endf	Isotope	J
-0.98	0.02	[0.007]	-1.2400	90	7	[0.6]	86.70	1.7	0.1	[0.02]	3.0600	153	2
-0.0104	0.0004	[0.0009]	-0.0609	80	0.3	[10]	105.20	0.013	0.0004	[0.003]	0.0768	151	3
0.3273	0.0003	[0.0004]	0.3210	125	0.4	[1]	79.50	0.094	0.0009	[0.001]	0.0714	151	3
0.4650	0.0002	[0.0001]	0.4600	94.5	0.4	[0.3]	87.00	0.72	0.004	[0.01]	0.6651	151	3
1.0543	0.0001	[0.0007]	1.0550	85.1	0.3	[0.9]	88.00	0.2132	0.0004	[0.0007]	0.1932	151	3
1.7233	0.0002	[0.0003]	1.7270	94.4	0.6	[0.5]	90.00	0.0654	0.0002	[0.0004]	0.0684	153	2
1.806	0.001	[0.0005]	1.8150	95	3	[3]	91.00	0.037	0.0006	[0.001]	0.0408	151	2
2.4581	0.0001	[0.0001]	2.4560	96	0.4	[1]	91.00	1.180	0.003	[0.009]	1.0286	153	3
2.717	0.0005	[0.002]	2.7170	90	1	[1]	94.00	0.212	0.001	[0.001]	0.2057	151	3
3.2946	0.0001	[0.0002]	3.2940	96.8	0.3	[0.7]	98.00	1.21	0.003	[0.01]	1.0920	153	2
3.370	0.0003	[0.002]	3.3680	87	0.5	[1]	93.00	2.62	0.009	[0.01]	2.1960	151	2
3.711	0.0004	[0.002]	3.7100	91	1	[0.5]	93.00	1.037	0.005	[0.002]	0.9480	151	2
3.9429	0.0001	[0.0002]	3.9440	94.8	0.4	[0.4]	93.00	1.41	0.003	[0.01]	1.3200	153	2
4.767	0.001	[0.0008]	4.7500	97	4	[3]	91.00	0.0314	0.0005	[0.0006]	0.0317	153	3
4.796	0.003	[0.002]	4.7900	66	5	[2]	91.00	0.036	0.001	[0.002]	0.1800	151	2
5.382	0.0008	[0.002]	5.3800	79	2	[2]	108.00	0.159	0.002	[0.0009]	0.1517	151	3
5.975	0.001	[0.002]	5.9800	110	3	[2]	100.00	0.210	0.003	[0.004]	0.3000	151	3
6.1594	0.0003	[0.0001]	6.1600	100.2	0.6	[0.5]	104.00	0.554	0.002	[0.003]	0.5571	153	3
7.010	0.002	[0.004]	7.0500	82	4	[2]	91.00	0.41	0.02	[0.006]	0.0636	151	2
7.225	0.0009	[0.005]	7.2900	85	3	[2]	88.00	1.74	0.03	[0.002]	1.8857	151	3
7.426	0.0008	[0.005]	7.4400	83	1	[1]	85.00	2.75	0.02	[0.001]	1.6286	151	3
8.8632	0.0002	[0.0004]	8.8500	91	0.5	[1]	101.00	5.01	0.02	[0.05]	4.3200	153	2
9.069	0.002	[0.006]	9.0700	84	3	[4]	104.00	0.91	0.01	[0.007]	1.2480	151	2
10.4639	0.0006	[0.0009]	10.4700	100			91.00	2.88	0.01	[0.01]	2.4840	151	2
10.947	0.002	[0.002]	10.9400	100			98.00	0.361	0.004	[0.003]	0.5657	151	3
11.6243	0.0003	[0.0003]	11.6100	110			94.00	3.64	0.02	[0.05]	3.3857	153	3
12.200	0.001	[0.02]	12.2300	100			88.00	1.11	0.01	[0.007]	1.1280	151	2
12.454	0.002	[0.02]	12.4500	110			81.00	0.142	0.002	[0.001]	0.1200	153	3
12.524	0.002	[0.02]	NEW	100			NEW	0.87	0.02	[0.009]	NEW	151	3
12.701	0.001	[0.01]	12.6400	100			88.00	2.04	0.03	[0.02]	2.8800	151	2
13.2333	0.0009	[0.0005]	13.2200	110			90.00	0.508	0.004	[0.003]	0.3840	153	2
13.683	0.002	[0.02]	13.6600	100			115.00	0.393	0.005	[0.002]	0.3771	151	3
14.760	0.0009	[0.02]	14.7600	100			76.00	3.13	0.02	[0.02]	2.3040	151	2
15.192	0.0009	[0.003]	15.1800	100			79.00	3.23	0.02	[0.06]	2.5200	151	2
15.295	0.001	[0.001]	15.2600	110			110.00	0.397	0.004	[0.003]	0.3240	153	2
16.13	0.04	[0.001]	16.3300	110			90.00	0.0066	0.0007	[0.0001]	0.0206	153	3
16.7288	0.0007	[0.0006]	16.7300	110			103.00	1.76	0.01	[0.02]	1.6320	153	2
17.566	0.003	[0.004]	17.6000	110			90.00	0.332	0.006	[0.004]	0.6600	153	2
17.734	0.002	[0.004]	17.7500	100			104.00	1.62	0.02	[0.02]	1.6200	151	2
18.0221	0.0005	[0.0008]	18.0100	110			90.00	4.18	0.02	[0.06]	3.9429	153	3
18.758	0.0006	[0.002]	18.7300	110			110.00	3.75	0.002	[0.02]	3.3600	153	2
19.111	0.001	[0.002]	19.1000	100			133.00	4.68	0.003	[0.03]	4.2686	151	3
20.0229	0.0004	[0.0007]	20.0200	110			109.00	18.9	0.09	[0.2]	11.7600	153	2
21.682	0.002	[0.003]	21.6900	100			82.00	1.83	0.02	[0.01]	1.6800	151	3
22.205	0.001	[0.002]	22.2100	100			66.00	3.70	0.03	[0.03]	2.4429	151	3
22.5439	0.0007	[0.0007]	22.5400	110			88.00	3.10	0.02	[0.02]	3.0000	153	2
22.737	0.003	[0.004]	22.7500	100			89.00	1.23	0.02	[0.02]	1.3114	151	3
23.6669	0.0008	[0.0009]	23.6600	110			86.00	2.40	0.02	[0.01]	2.4000	153	3
24.266	0.003	[0.004]	NEW	100			NEW	1.75	0.03	[0.02]	NEW	151	2
24.592	0.001	[0.002]	24.5800	100			99.00	5.34	0.04	[0.05]	6.8143	151	3
25.210	0.003	[0.002]	25.1700	100			91.00	1.07	0.02	[0.007]	0.7200	151	2
25.612	0.005	[0.005]	25.6000	100			89.00	0.68	0.02	[0.003]	0.6120	151	2
26.160	0.005	[0.005]	26.1900	110			90.00	0.170	0.005	[0.003]	0.2229	153	3
26.709	0.001	[0.003]	26.7200	100			78.00	11.48	0.07	[0.07]	8.4000	151	2
27.481	0.006	[0.008]	27.4300	100			97.00	0.38	0.01	[0.004]	0.5400	151	3
28.043	0.008	[0.006]	28.0900	100			90.00	0.41	0.02	[0.005]	0.3840	151	2
28.659	0.001	[0.001]	28.6300	110			73.00	1.71	0.01	[0.01]	1.4571	153	3
29.248	0.002	[0.002]	29.2300	100			79.00	6.12	0.05	[0.04]	5.4480	151	2
29.965	0.006	[0.003]	29.9000	110			90.00	0.284	0.008	[0.002]	0.2314	153	3
30.244	0.004	[0.0008]	30.2200	100			86.00	4.9	0.1	[0.03]	4.3440	151	2
30.77	0.02	[0.001]	30.8100	100			99.00	0.63	0.04	[0.02]	0.5743	151	3
31.246	0.007	[0.003]	31.2200	110			117.00	2.38	0.09	[0.03]	1.9714	153	3
31.621	0.007	[0.001]	31.5900	100			97.00	2.3	0.08	[0.1]	2.0400	151	2
32.48	0.05	[0.01]	32.4500	110			93.34	0.39	0.04	[0.003]	0.2760	153	2
33.48	0.03	[0.005]	33.5100	100			91.00	0.39	0.03	[0.009]	0.3943	151	3
34.529	0.004	[0.002]	34.5300	110			90.00	7.3	0.2	[0.1]	6.2400	153	2
34.94	0.05	[0.02]	34.5700	100			91.00	0.35	0.04	[0.001]	0.3000	151	3
35.098	0.007	[0.005]	35.0500	100			90.00	3.4	0.1	[0.06]	3.8400	151	2
36.089	0.004	[0.003]	36.0900	100			78.00	4.8	0.1	[0.1]	4.3286	151	3
36.632	0.006	[0.003]	36.6200	110			106.00	5.4	0.2	[0.2]	5.0400	153	2
37.031	0.004	[0.0008]	37.0100	100			78.00	9.5	0.2	[0.08]	6.7200	151	2
37.768	0.006	[0.009]	37.7600	110			94.00	4.4	0.1	[0.04]	3.7714	153	3

(*continued on next page*)

Table 4 (*continued*)

E,eV	ΔE Bayesian	[external]	Eendf	$\Gamma\gamma$	$\Delta\Gamma_\gamma$ Bayesian	[external]	$\Gamma_\gamma$endf	Γ_n	$\Delta\Gamma_n$ Bayesian	[external]	$\Gamma_n$endf	Isotope	J
37.77	0.008	[0.02]	37.7800	100			92.00	2.7	0.1	[0.05]	2.9486	151	3
38.309	0.005	[0.005]	38.3000	110			81.00	8.2	0.2	[0.3]	7.0800	153	2
38.97	0.02	[0.02]	39.2000	100			91.00	1.4	0.1	[0.02]	1.2000	151	2
39.290	0.005	[0.0006]	39.3700	100			79.00	4.6	0.1	[0.04]	3.4457	151	3
39.96	0.01	[0.01]	39.9400	100			79.00	1.15	0.07	[0.06]	1.0800	151	3
41.19	0.02	[0.03]	41.1500	110			69.00	1.5	0.1	[0.03]	1.6800	153	2
41.385	0.002	[0.005]	41.3500	115	5 [3]		80.00	28.4	0.5	[0.7]	32.4000	151	2
42.04	0.03	[0.04]	42.1200	100			91.00	1.06	0.09	[0.01]	1.2480	151	2
42.19	0.006	[0.01]	42.1500	110			77.00	6.8	0.2	[0.2]	5.7600	153	2
43.191	0.009	[0.006]	43.1600	110			96.00	3.3	0.1	[0.06]	2.7429	153	3
43.20	0.006	[0.01]	43.1900	100			84.00	4.7	0.1	[0.1]	4.8429	151	3
44.44	0.007	[0.01]	44.4300	100			89.00	4.4	0.2	[0.06]	4.3200	151	2
44.93	0.04	[0.01]	44.8200	110			93.34	0.89	0.08	[0.01]	0.8040	153	2
45.43	0.02	[0.07]	45.4200	100			99.00	1.6	0.1	[0.02]	1.6200	151	2
45.81	0.02	[0.01]	45.7900	110			99.00	1.4	0.1	[0.01]	1.2000	153	3
46.397	0.003	[0.001]	46.4100	85	5 [6]		85.00	27.0	0.4	[0.5]	12.4800	151	2
47.06	0.02	[0.0009]	47.1100	110			94.00	1.7	0.1	[0.04]	1.8000	153	3
47.098	0.004	[0.002]	47.2400	100			99.00	11.5	0.3	[0.2]	14.5714	151	3
47.42	0.03	[0.006]	NEW	100			NEW	2.3	0.2	[0.06]	NEW	151	2
47.900	0.006	[0.004]	47.9300	110			93.34	9.4	0.3	[0.006]	7.4400	153	2
49.2	0.1	[0.001]	49.3000	110			93.34	0.15	0.01	[0.0007]	0.1200	153	3
49.26	0.09	[0.06]	49.5000	110			93.34	0.54	0.05	[0.006]	0.3360	153	2
49.98	0.01	[0.004]	50.0000	110			92.00	2.6	0.1	[0.02]	2.5714	153	3
50.03	0.02	[0.009]	50.0400	100			91.00	1.7	0.1	[0.03]	0.8486	151	3
50.656	0.004	[0.008	50.5800	100			102.00	15.7	0.4	[0.3]	19.7143	151	3
50.757	0.006	[0.006]	50.7400	110			113.00	10.4	0.3	[0.2]	8.8800	153	2
52.15	0.02	[0.02]	52.3100	100			108.00	2.8	0.2	[0.08]	10.2857	151	3
52.326	0.004	[0.002]	52.4100	110			91.00	13.4	0.3	[0.2]	3.4714	153	3
52.61	0.01	[0.01]	52.7000	100			80.00	5.6	0.3	[0.09]	5.7600	151	2
53.10	0.01	[0.004]	53.0700	110			119.00	3.0	0.2	[0.1]	2.4000	153	3
53.33	0.04	[0.04]	53.2500	100			91.00	0.71	0.06	[0.01]	0.7543	151	3
53.94	0.01	[0.02]	53.9400	100			88.00	4.3	0.2	[0.08]	5.5200	151	2
54.279	0.004	[0.003]	54.2900	110			93.34	19.6	0.5	[0.5]	14.4000	153	2
55.28	0.01	[0.008]	55.1900	100			95.00	3.5	0.1	[0.07]	0.3600	151	3
55.5	0.1	[0.03]	55.2600	110			96.00	0.35	0.04	[0.0008]	3.3429	153	2
55.56	0.03	[0.02]	55.5700	110			93.34	1.4	0.1	[0.02]	1.6286	153	3
56.16	0.02	[0.03]	56.1800	100			98.00	1.7	0.1	[0.04]	3.0000	151	3
57.18	0.01	[0.01]	NEW	100			NEW	7.2	0.4	[0.3]	NEW	151	2
57.505	0.008	[0.007]	57.3600	100			83.00	8.5	0.3	[0.3]	16.2857	151	3
58.829	0.008	[0.005]	58.8500	100			108.00	5.7	0.2	[0.3]	5.4857	151	3
59.07	0.04	[0.07]	58.9700	110			85.00	1.4	0.1	[0.03]	1.4400	153	2
59.76	0.02	[0.01]	59.7200	110			102.00	3.3	0.2	[0.06]	3.3600	153	2
60.70	0.02	[0.03]	60.8500	100			96.00	4.7	0.3	[0.3]	6.9600	151	2
60.903	0.005	[0.002]	60.9200	129	8 [9]		78.00	27	0.7	[2]	38.4000	153	2
62.46	0.01	[0.02]	62.4100	100			86.00	3.2	0.2	[0.04]	3.4286	151	3
62.55	0.02	[0.02]	62.5500	110			105.00	2.8	0.2	[0.04]	4.2857	153	3
63.12	0.02	[0.01]	63.1900	100			100.00	3.1	0.2	[0.1]	2.1429	151	3
63.71	0.007	[0.01]	63.7000	110			93.00	20.4	0.7	[0.7]	6.2571	153	3
64.09	0.007	[0.01]	64.0900	110			116.00	20.2	0.7	[0.3]	12.0000	153	3
65.49	0.02	[0.006]	NEW	100			NEW	2.8	0.2	[0.04]	NEW	151	2
67.05	0.03	[0.02]	66.9400	110			86.00	2.4	0.2	[0.01]	3.2571	153	3
67.929	0.006	[0.007]	67.9100	100			100.00	13.0	0.3	[0.4]	15.4286	151	3
68.21	0.01	[0.006]	68.1500	110			87.00	7.3	0.4	[0.4]	6.1200	153	2
68.98	0.05	[0.06]	69.0900	100			91.00	1.1	0.1	[0.02]	1.2000	151	2
70.04	0.02	[0.02]	70.0400	110			100.00	3.0	0.2	[0.05]	2.5714	153	3
70.78	0.01	[0.007]	70.7500	100			78.00	5.6	0.3	[0.03]	5.4000	151	2
70.99	0.07	[0.03]	71.3500	110			93.34	1.2	0.1	[0.005]	1.4400	153	2
71.47	0.01	[0.009]	71.4100	100			84.00	8.5	0.3	[0.2]	7.3200	151	2
72.42	0.03	[0.02]	72.4100	100			93.00	1.7	0.1	[0.02]	1.8857	151	3
73.45	0.04	[0.03]	73.3300	100			91.00	1.1	0.1	[0.02]	1.0286	151	3
73.4	0.1	[0.03]	73.6800	110			93.34	0.32	0.03	[0.0004]	0.2914	153	3
74.15	0.04	[0.03]	74.1600	100			91.00	1.1	0.1	[0.02]	1.3714	151	3
75.6	0.1	[0.03]	75.4700	110			93.34	0.52	0.05	[0.003]	0.4457	153	3
75.79	0.02	[0.01]	75.7600	100			90.00	4.7	0.3	[0.06]	5.0400	151	2
76.92	0.009	[0.02]	76.9300	110			105.00	11.2	0.4	[0.2]	12.0000	153	3
77.43	0.01	[0.02]	77.4500	100			99.00	7.0	0.3	[0.1]	7.5429	151	3
77.81	0.08	[0.06]	78.0500	100			91.00	0.69	0.07	[0.009]	0.4543	151	3
78.64	0.01	[0.02]	78.6600	100			73.00	8.0	0.5	[0.04]	14.5714	151	3
78.83	0.02	[0.01]	NEW	100			NEW	6.7	0.5	[0.05]	NEW	151	3
79.53	0.01	[0.01]	79.5100	100			64.00	5.3	0.2	[0.04]	4.7143	151	3
80.25	0.03	[0.02]	80.2900	110			81.00	3.3	0.2	[0.05]	9.8400	153	3
80.34	0.01	[0.005]	80.2900	100			103.00	10.3	0.4	[0.4]	4.1143	151	2
81.051	0.006	[0.002]	81.0800	100			101.00	20.4	0.5	[0.3]	20.5714	151	3
81.32	0.02	[0.02]	81.2400	110			96.00	5.0	0.3	[0.2]	4.8000	153	2

(*continued on next page*)

Table 4 (*continued*)

E,eV	ΔE Bayesian	[external]	Eendf	$\Gamma\gamma$	$\Delta\Gamma_\gamma$ Bayesian	[external]	$\Gamma_\gamma$endf	Γ_n	$\Delta\Gamma_n$ Bayesian	[external]	$\Gamma_n$endf	Isotope	J
83.04	0.03	[0.01]	82.9900	110			86.00	3.4	0.2	[0.09]	3.0857	153	3
83.09	0.03	[0.003]	83.0700	100			95.00	2.4	0.2	[0.02]	2.8286	151	3
83.85	0.02	[0.01]	84.0000	100			99.00	7.9	0.6	[0.2]	18.0000	151	2
84.19	0.02	[0.02]	NEW	100			NEW	5.9	0.4	[0.1]	NEW	151	3
84.5	0.1	[0.03]	84.0000	110			93.34	0.68	0.07	[0.001]	0.6257	153	3
85.68	0.02	[0.003]	85.6700	100			84.00	4.4	0.2	[0.1]	4.1143	151	3
86.94	0.01	[0.009]	86.9900	110			68.00	10.8	0.4	[0.4]	10.2857	153	3
87.49	0.07	[0.06]	87.7000	100			91.00	1.5	0.1	[0.02]	1.5600	151	2
87.74	0.03	[0.07]	87.7000	110			105.00	5.2	0.4	[0.1]	5.8800	153	2
88.4	0.04	[0.1]	88.6300	100			91.00	1.9	0.2	[0.03]	0.9429	151	3
89.35	0.02	[0.07]	89.3400	100			104.00	8.7	0.4	[0.2]	12.8571	151	3
89.4	0.1	[0.03]	89.3400	110			93.34	1.6	0.2	[0.002]	1.5600	153	2
90.23	0.02	[0.06]	90.1800	100			85.00	6.0	0.4	[0.2]	5.8800	151	2
90.84	0.04	[0.06]	90.7500	110			79.00	4.3	0.3	[0.03]	5.0400	153	2
91.17	0.02	[0.02]	91.1300	100			94.00	5.3	0.3	[0.1]	5.7600	151	2
92.95	0.07	[0.01]	92.8000	110			93.34	2.0	0.2	[0.006]	1.9714	153	3
93.275	0.006	[0.004]	93.2600	79	6 [0.4]]		88.00	33	1	[2]	36.0000	153	3
93.35	0.01	[0.01]	93.3600	110	10 [0.4]		112.00	25	1	[1]	33.6000	151	2
93.97	0.02	[0.01]	NEW	100			NEW	4.8	0.3	[0.07]	NEW	151	3
93.8	0.1	[0.03]	94.7600	110			93.34	0.65	0.06	[0.001]	0.6686	153	3
94.91	0.07	[0.03]	95.1500	110			93.34	1.9	0.2	[0.02]	2.7600	153	2
95.93	0.03	[0.009]	NEW	100			NEW	5.0	0.4	[0.04]	NEW	151	2
96.34	0.01	[0.004]	96.2900	100			112.00	10.4	0.4	[0.1]	16.2857	151	3
96.54	0.06	[0.02]	NEW	100			NEW	2.7	0.2	[0.02]	NEW	151	2
96.88	0.04	[0.01]	96.8600	110			93.34	3.0	0.2	[0.08]	2.5714	153	3
97.62	0.01	[0.02]	97.6000	110			101.00	14.7	0.7	[0.6]	22.2857	153	3
97.77	0.08	[0.04]	97.7000	100			91.00	1.6	0.1	[0.004]	1.8857	151	3
98.02	0.06	[0.02]	NEW	110			NEW	3.7	0.4	[0.07]	NEW	153	2
98.63	0.01	[0.02]	98.6100	100			108.00	19.4	0.7	[0.8]	19.2000	151	2
100.52	0.03	[0.05]	NEW	110			NEW	5.4	0.4	[0.1]	NEW	153	UNASSIGNED
100.72	0.01	[0.007]	NEW	100			NEW	16	0.6	[1]	NEW	151	UNASSIGNED
102.283	0.009	[0.009]	NEW	120	10 [1]		NEW	25.3	0.9	[0.7]	NEW	153	UNASSIGNED
102.70	0.01	[0.004]	NEW	100			NEW	13.3	0.6	[0.1]	NEW	151	UNASSIGNED
104.14	0.02	[0.02]	NEW	100			NEW	7.7	0.4	[0.2]	NEW	151	UNASSIGNED
105.01	0.07	[0.07]	NEW	110			NEW	2.6	0.3	[0.02]	NEW	153	UNASSIGNED
105.34	0.02	[0.008]	NEW	110			NEW	10.7	0.7	[0.2]	NEW	153	UNASSIGNED
105.93	0.03	[0.02]	NEW	110			NEW	6.5	0.5	[0.2]	NEW	153	UNASSIGNED
106.79	0.02	[0.005]	NEW	100			NEW	8.5	0.4	[0.2]	NEW	151	UNASSIGNED
107.46	0.02	[0.04]	NEW	110			NEW	9.5	0.6	[0.2]	NEW	153	UNASSIGNED
107.86	0.03	[0.02]	NEW	100			NEW	6.2	0.4	[0.2]	NEW	151	UNASSIGNED
108.34	0.07	[0.08]	NEW	110			NEW	2.2	0.2	[0.02]	NEW	153	UNASSIGNED
109.09	0.02	[0.03]	NEW	100			NEW	13.5	0.8	[0.2]	NEW	151	UNASSIGNED
109.51	0.02	[0.02]	NEW	100			NEW	12.5	0.8	[0.09]	NEW	151	UNASSIGNED
110.22	0.01	[0.02]	NEW	100			NEW	16.0	0.6	[0.2]	NEW	151	UNASSIGNED
111.23	0.04	[0.03]	NEW	100			NEW	5.7	0.5	[0.03]	NEW	151	UNASSIGNED
111.64	0.01	[0.01]	NEW	107	9 [0.9]		NEW	27	0.9	[1]	NEW	151	UNASSIGNED
112.82	0.05	[0.04]	NEW	100			NEW	2.7	0.2	[0.05]	NEW	151	UNASSIGNED
113.7	0.03	[0.1]	NEW	100			NEW	4.7	0.3	[0.06]	NEW	151	UNASSIGNED
114.31	0.02	[0.02]	NEW	100			NEW	10.7	0.5	[0.3]	NEW	151	UNASSIGNED
115.38	0.02	[0.01]	NEW	100			NEW	6.6	0.4	[0.2]	NEW	151	UNASSIGNED
116.04	0.07	[0.08]	NEW	110			NEW	2.6	0.2	[0.01]	NEW	153	UNASSIGNED
116.86	0.03	[0.02]	NEW	100			NEW	7.0	0.5	[0.2]	NEW	151	UNASSIGNED
117.24	0.02	[0.002]	NEW	110			NEW	14.1	0.8	[0.1]	NEW	153	UNASSIGNED
118.02	0.04	[0.04]	NEW	110			NEW	6.5	0.5	[0.2]	NEW	153	UNASSIGNED
119.02	0.06	[0.04]	NEW	110			NEW	3.8	0.3	[0.006]	NEW	153	UNASSIGNED
120.30	0.02	[0.05]	NEW	110	10 [2]		NEW	17	0.8	[3]	NEW	151	UNASSIGNED
121.10	0.04	[0.07]	NEW	100			NEW	7.2	0.5	[0.2]	NEW	151	UNASSIGNED
121.61	0.02	[0.003]	NEW	110			NEW	16.9	0.9	[0.4]	NEW	153	UNASSIGNED
121.63	0.04	[0.01]	NEW	100			NEW	5.8	0.5	[0.09]	NEW	151	UNASSIGNED
122.9	0.1	[0.03]	NEW	110			NEW	2.0	0.2	[0.01]	NEW	153	UNASSIGNED
123.91	0.06	[0.08]	NEW	110			NEW	3.4	0.3	[0.04]	NEW	153	UNASSIGNED
124.64	0.03	[0.02]	NEW	100			NEW	5.8	0.4	[0.2]	NEW	151	UNASSIGNED
125.03	0.08	[0.09]	NEW	110			NEW	2.5	0.2	[0.02]	NEW	153	UNASSIGNED
125.46	0.09	[0.05]	NEW	110			NEW	2.5	0.2	[0.008]	NEW	153	UNASSIGNED
125.65	0.07	[0.01]	NEW	100			NEW	2.2	0.2	[0.02]	NEW	151	UNASSIGNED
126.8	0.1	[0.06]	NEW	110			NEW	1.2	0.1	[0.01]	NEW	153	UNASSIGNED
127.53	0.07	[0.04]	NEW	110			NEW	3.3	0.3	[0.03]	NEW	153	UNASSIGNED
127.56	0.03	[0.01]	NEW	100			NEW	6.2	0.4	[0.04]	NEW	151	UNASSIGNED
128.1	0.1	[0.04]	NEW	110			NEW	1.4	0.1	[0.009]	NEW	153	UNASSIGNED
129.1	0.09	[0.1]	NEW	110			NEW	2.2	0.2	[0.04]	NEW	153	UNASSIGNED
129.12	0.01	[0.007]	NEW	99	9 [0.6]		NEW	19.6	0.8	[0.7]	NEW	151	UNASSIGNED
130.49	0.05	[0.01]	NEW	100			NEW	3.0	0.3	[0.02]	NEW	151	UNASSIGNED
130.87	0.09	[0.05]	NEW	110			NEW	2.3	0.2	[0.006]	NEW	153	UNASSIGNED
131.35	0.03	[0.03]	NEW	100			NEW	6.3	0.5	[0.2]	NEW	151	UNASSIGNED

(*continued on next page*)

Table 4 (*continued*)

E,eV	ΔE Bayesian	[external]	Eendf	$\Gamma\gamma$	$\Delta\Gamma_\gamma$ Bayesian	[external]	$\Gamma_\gamma$endf	Γ_n	$\Delta\Gamma_n$ Bayesian	[external]	$\Gamma_n$endf	Isotope	J
133.72	0.09	[0.07]	NEW	100			NEW	2.9	0.3	[0.08]	NEW	151	UNASSIGNED
133.92	0.08	[0.08]	NEW	100			NEW	4.2	0.4	[0.1]	NEW	151	UNASSIGNED
134.60	0.05	[0.03]	NEW	100			NEW	4.4	0.4	[0.2]	NEW	151	UNASSIGNED
135.06	0.08	[0.09]	NEW	110			NEW	2.6	0.2	[0.05]	NEW	153	UNASSIGNED
137.4	0.1	[0.06]	NEW	110			NEW	1.9	0.2	[0.02]	NEW	153	UNASSIGNED
138.66	0.08	[0.06]	NEW	110			NEW	3.5	0.3	[0.07]	NEW	153	UNASSIGNED
139.96	0.03	[0.009]	NEW	100			NEW	10.2	0.7	[0.5]	NEW	151	UNASSIGNED
140.37	0.03	[0.01]	NEW	110			NEW	12.6	0.8	[0.8]	NEW	153	UNASSIGNED
141.03	0.02	[0.03]	NEW	110	10 [1]		NEW	23	1	[1]	NEW	151	UNASSIGNED
142.08	0.03	[0.02]	NEW	100			NEW	8.9	0.6	[0.2]	NEW	151	UNASSIGNED
143.1	0.2	[0.06]	NEW	110			NEW	1.2	0.1	[0.006]	NEW	153	UNASSIGNED
144.18	0.02	[0.04]	NEW	100			NEW	12.7	0.8	[0.2]	NEW	151	UNASSIGNED
144.7	0.1	[0.05]	NEW	110			NEW	3.2	0.3	[0.009]	NEW	153	UNASSIGNED
144.91	0.04	[0.03]	NEW	100			NEW	9.4	0.8	[0.1]	NEW	151	UNASSIGNED
145.07	0.05	[0.004]	NEW	110			NEW	7.0	0.6	[0.03]	NEW	153	UNASSIGNED
145.3	0.2	[0.02]	NEW	100			NEW	2.6	0.3	[0.01]	NEW	151	UNASSIGNED
145.77	0.02	[0.02]	NEW	100	10 [0.8]		NEW	22	1	[0.4]	NEW	151	UNASSIGNED
146.21	0.03	[0.04]	NEW	110			NEW	13.2	0.8	[0.2]	NEW	153	UNASSIGNED
146.85	0.03	[0.02]	NEW	100			NEW	7.1	0.5	[0.1	NEW	151	UNASSIGNED
148.22	0.02	[0.01]	NEW	100			NEW	12.3	0.7	[0.3]	NEW	151	UNASSIGNED
149.4	0.1	[0.02]	NEW	100			NEW	1.5	0.2	[0.01]	NEW	151	UNASSIGNED
150.47	0.03	[0.04]	NEW	110			NEW	12.3	0.9	[0.2]	NEW	153	UNASSIGNED
151.1	0.1	[0.03]	NEW	110			NEW	3.3	0.3	[0.03]	NEW	153	UNASSIGNED
151.92	0.03	[0.04]	NEW	100			NEW	13.3	0.8	[0.4]	NEW	151	UNASSIGNED
152.66	0.05	[0.06]	NEW	100			NEW	7.8	0.6	[0.2]	NEW	151	UNASSIGNED
152.73	0.03	[0.04]	NEW	110			NEW	10.7	0.8	[0.03]	NEW	153	UNASSIGNED
153.96	0.01	[0.01]	NEW	110	10 [0.8]		NEW	28	1	[1]	NEW	151	UNASSIGNED
154.83	0.04	[0.05]	NEW	110			NEW	10.4	0.8	[0.09]	NEW	153	UNASSIGNED
155.15	0.02	[0.02]	NEW	110	10 [0.6]		NEW	29	1	[0.5]	NEW	151	UNASSIGNED
156.34	0.01	[0.01]	NEW	140	10 [3]		NEW	72	3	[5]	NEW	153	UNASSIGNED
156.81	0.04	[0.02]	NEW	110			NEW	14	1	[0.1]	NEW	153	UNASSIGNED
158.30	0.04	[0.02]	NEW	100			NEW	7.1	0.5	[0.08]	NEW	151	UNASSIGNED
159.16	0.06	[0.05]	NEW	100			NEW	5.2	0.4	[0.02]	NEW	151	UNASSIGNED
159.70	0.05	[0.03]	NEW	110			NEW	8.2	0.7	[0.2]	NEW	153	UNASSIGNED
160.61	0.03	[0.004]	NEW	110			NEW	16	1	[0.5]	NEW	153	UNASSIGNED
162.02	0.02	[0.04]	NEW	100			NEW	12.6	0.7	[0.4]	NEW	151	UNASSIGNED
163.39	0.04	[0.03]	NEW	100			NEW	8.6	0.7	[0.03]	NEW	151	UNASSIGNED
164.1	0.09	[0.1]	NEW	100			NEW	3.3	0.3	[0.06]	NEW	151	UNASSIGNED
165.98	0.03	[0.05]	NEW	100			NEW	10.1	0.7	[0.2]	NEW	151	UNASSIGNED
166.85	0.02	[0.009]	NEW	110	10 [0.9]		NEW	18	1	[0.6]	NEW	151	UNASSIGNED
168.53	0.03	[0.04]	NEW	100			NEW	12.1	0.8	[0.04]	NEW	151	UNASSIGNED
169.45	0.02	[0.04]	NEW	110	10 [0.7]		NEW	23	1	[1]	NEW	151	UNASSIGNED
169.84	0.07	[0.01]	NEW	110			NEW	6.8	0.6	[0.1]	NEW	153	UNASSIGNED
170.29	0.05	[0.08]	NEW	110			NEW	8.9	0.8	[0.3]	NEW	153	UNASSIGNED
172.61	0.05	[0.02]	NEW	100			NEW	6.4	0.5	[0.2]	NEW	151	UNASSIGNED
174.15	0.06	[0.02]	NEW	100			NEW	4.2	0.4	[0.2]	NEW	151	UNASSIGNED
175.84	0.02	[0.006]	NEW	120	10 [0.5]		NEW	30	2	[0.6]	NEW	153	UNASSIGNED
176.34	0.02	[0.05]	NEW	99	9 [2]		NEW	37	2	[0.3]	NEW	151	UNASSIGNED
177.04	0.03	[0.04]	NEW	100	10 [0.5]		NEW	22	2	[1]	NEW	151	UNASSIGNED
178.54	0.03	[0.04]	NEW	110			NEW	17	1	[0.5]	NEW	153	UNASSIGNED
180.08	0.02	[0.03]	NEW	100	10 [0.6]		NEW	18	1	[0.3]	NEW	151	UNASSIGNED
181.49	0.02	[0.03]	NEW	100	10 [0.7]		NEW	21	1	[0.3]	NEW	151	UNASSIGNED
183.16	0.02	[0.003]	NEW	120	10 [0.7]		NEW	32	2	[0.9]	NEW	153	UNASSIGNED
184.31	0.02	[0.03]	NEW	120	10 [2]		NEW	44	2	[1]	NEW	153	UNASSIGNED
185.00	0.02	[0.02]	NEW	110	10 [0.7]		NEW	27	1	[0.7]	NEW	151	UNASSIGNED
186.53	0.02	[0.03]	NEW	100	1 [0.5] 0		NEW	20	1	[0.8]	NEW	151	UNASSIGNED
187.72	0.03	[0.03]	NEW	100			NEW	17	1	[0.4]	NEW	151	UNASSIGNED
188.73	0.02	[0.03]	NEW	110	10 [2]		NEW	30	1	[2]	NEW	151	UNASSIGNED
190.42	0.04	[0.01]	NEW	110			NEW	14	1	[0.1]	NEW	153	UNASSIGNED
192.4	0.09	[0.2]	NEW	100			NEW	8.6	0.8	[0.1]	NEW	151	UNASSIGNED
192.17	0.03	[0.05]	NEW	110	10 [0.6]		NEW	27	2	[0.1]	NEW	153	UNASSIGNED
192.6	0.1	[0.1]	NEW	110			NEW	7.0	0.7	[0.07]	NEW	153	UNASSIGNED
193.20	0.03	[0.01]	NEW	90	10 [0.6]		NEW	30	2	[2]	NEW	151	UNASSIGNED
193.6	0.06	[0.1]	NEW	110			NEW	10.6	0.9	[0.3]	NEW	153	UNASSIGNED
195.0	0.1	[0.06]	NEW	110			NEW	4.5	0.4	[0.05]	NEW	153	UNASSIGNED
195.95	0.05	[0.04]	NEW	100			NEW	12	1	[0.1]	NEW	151	UNASSIGNED
196.66	0.03	[0.004]	NEW	100	10 [0.6]		NEW	26	2	[0.2]	NEW	151	UNASSIGNED
197.4	0.1	[0.04]	NEW	110			NEW	5.4	0.5	[0.03]	NEW	153	UNASSIGNED
198.45	0.07	[0.04]	NEW	100			NEW	6.4	0.5	[0.2]	NEW	151	UNASSIGNED
199.38	0.07	[0.06]	NEW	110			NEW	7.5	0.7	[0.05]	NEW	153	UNASSIGNED

4.2. Details of the SAMMY analysis

Resonance parameters were extracted from transmission and capture data using the R-matrix Bayesian computer code SAMMY. The results are presented in Table 4. The present analysis assumed the same spin assignments as ENDF/B-VII.1. For newly identified resonances spin was assigned based on the best fit. Above 100 eV the spin states were left unassigned. There are no p-wave resonances listed in ENDF in the resolved resonance region. No new p-wave resonances were assumed up to 200 eV. Other important aspects of the analysis included background in transmission, flux normalization in capture, zero-time measurement, and the experimental resolution function. Each of these aspects will be discussed in turn. No external R-function was employed.

4.3. Transmission background

Background was not fitted during the SAMMY analysis. However, the uncertainty in background was propagated into the final results. Background was accounted for in the data processing (described in Section 3.2.1) of each sample's counting spectrum before they were divided, producing transmission. Normalization was not varied in transmission fits.

4.4. Capture flux normalization

The neutron flux measurement and normalization for the capture experiment was described in Section 3.1. The capture flux normalization was never varied during the resonance parameter fitting with SAMMY.

4.5. Zero time measurement

The zero mark of each time-of-flight spectrum was observed as a peak in detector counts due to the gammas which accompany each pulse of neutrons. A separate measurement under each set of LINAC beam conditions was performed to identify the location, width, and shape of the neutron pulses.

4.6. Resolution function

Resolution broadening refers to the combined effects of the LINAC electron pulse width, the emission time in the moderator, the TOF channel width, and the effect of the detector system. The resolution function for thermal and epithermal capture, as well as epithermal transmission was characterized in SAMMY as a Gaussian distribution in time plus an exponential tail. The widths of the exponential tails of the distributions were fitted to measurements of depleted uranium (Barry, 2003; Leinweber et al., 2010). In the thermal transmission measurement the photomultiplier tube is in the neutron beam and must be represented by a more complex resolution function (Trbovich, 2003). A functional representation of the RPI resolution function was added to the SAMMY code in the late 1990s and continues to be used for thermal transmission data.

The flight path lengths for the various experiments are given in Table 1. The energy grid was determined by the epithermal capture measurement. Adjustments to flight path lengths for the epithermal and thermal transmission measurements and the thermal capture measurement were on the order of millimeters and are reflected in the propagated uncertainties discussed in Section 4.10.

4.7. Sample non-uniformity

Sample non-uniformity of thickness was determined from X-ray imaging of the samples as described in Section 2.2. A feature of the SAMMY program allows the input of areal density as a function of area fraction or radius. The tables of areal densities used in this analysis were taken from Ref. (Geuther et al., 2013). The effect of including the sample non-uniformities estimated from the X-ray imaging measurements was ≈3% on neutron width for the worst case, the thinnest sample. The 0.381-mm-thick ^{153}Eu-enriched sample was a stack of the 0.127- and 0.254-mm-thick samples. No areal density information was analyzed for the stacked sample.

The temperature used in the fits was 293 K. Due to the high purity of the samples, no impurities were included in the SAMMY analysis (see Table 3).

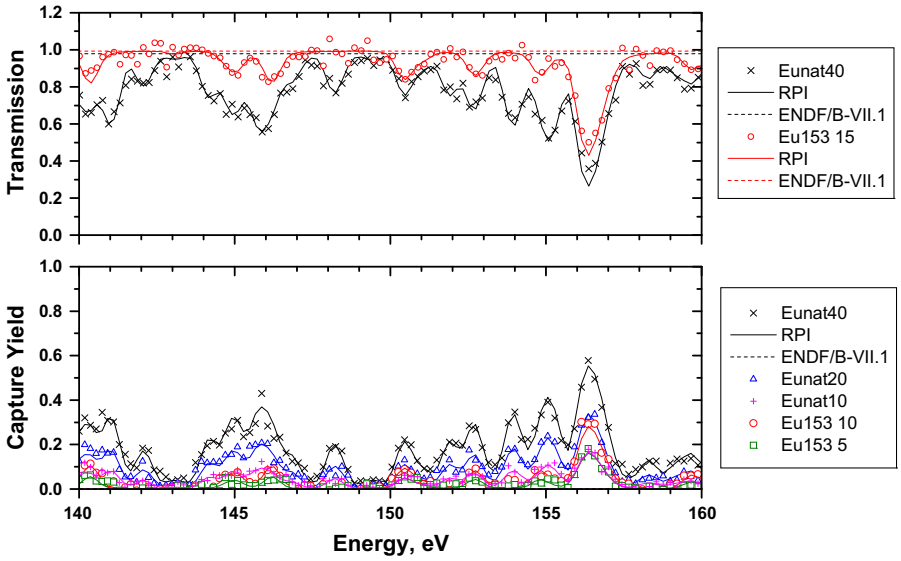

Fig. 7. Transmission and capture data from natural Eu and ^{153}Eu-enriched europium samples. The solid lines for all samples are the RPI parameters. The dashed lines for all samples are ENDF/B-VII.1. ENDF is a flat line with no structure above 100 eV. These measurements extend the resolved resonance region up to 200 eV. The figure gives an example of the current resonance treatment in the 140–160 eV region. Curve labels specify isotopic content (natural or ^{153}Eu-enriched), energy region (thermal or epithermal) and sample thickness (5, 10, 15, 20, or 40-mils), where one mil = 0.001 in. = 0.000254 cm.

4.8. Radiation width determination

For very low energy resonances, where the resolution width is small compared to the resonance total width, the radiation width was derived directly from the measured width of the resonance. At higher energy, radiation widths were determined whenever a resonance included a significant quantity of scattering. The criterion of $\Gamma_\gamma/\Gamma_n < 5$ was adopted from Ref. (Barry, 2003) to reflect sensitivity of a resonance to the value of the radiation width. Only for these resonances sensitive to the value of the radiation width, Γ_γ, is an uncertainty provided in the column labeled '$\Delta\Gamma_\gamma$' in Table 4; i.e., they satisfied the criterion.

For resonances with $\Gamma_\gamma/\Gamma_n > 5$, both transmission and capture measurements effectively measure the same quantity, Γ_n. For these mostly-capture resonances neither transmission nor capture data contain sufficient radiation width information. These resonances were assigned an average radiation width which was determined from all of the sensitive resonances with $\Gamma_\gamma/\Gamma_n < 5$. More detail on this method is given in Refs. (Barry, 2003; Leinweber et al., 2010). The average Γ_γ for each isotope, $<\Gamma_\gamma>$, is shown in Table 5. These values, obtained from all of the Γ_γ-sensitive resonances, were assigned to all of the Γ_γ-insensitive resonances in Table 4.

4.9. Resonance integrals and thermal total cross sections

Infinitely dilute capture resonance integrals (RIs) have been calculated from Eq. (3):

$$RI = \int_{0.5eV}^{20MeV} \sigma_C(E)\frac{dE}{E}, \quad (3)$$

where $\sigma_C(E)$ is the capture cross section in barns, Doppler broadened to 300 K, and E is energy in eV. The cross section was calculated from the resonance parameters shown in Table 4. Above 200 eV ENDF/B-VII.1 cross sections were used. The resonance integrals were calculated using the NJOY (MacFARLANE and Muir, 1994) and INTER (Dunford, 2001) programs. The results are shown in Table 6 in units of barns. Also, total thermal cross sections were calculated from resonance parameters using the NJOY and INTER programs, and the results are presented in Tables 6 and 7 including comparisons of the current measurements to ENDF/B-VII.1 (Chadwick et al., 2011), JEFF-3.1 (Santamarina et al., 2009) and JENDL-4.0 (Shibata et al., 2011) The capture resonance integral and thermal total cross section of ^{151}Eu have increased by (7 ± 1)% and (9 ± 3)%, respectively, compared to ENDF/B-VII.1. The capture resonance integral of ^{153}Eu has been raised by (9.9 ± 0.4)% relative to ENDF/B-VII.1, while thermal total cross section has decreased by (8 ± 3)%.

Changes in the ENDF library between release VII.0 (Chadwick et al., 2006) and VII.1 included a 0.8% increase in the capture resonance integral of ^{153}Eu and a 14% increase in the thermal total cross section of ^{153}Eu. The result of the current measurement of the thermal total cross section of ^{153}Eu lies between the values from ENDF/B-VII.0 and ENDF/F-B-VII.1.

The uncertainties in the resonance integrals given in Table 6 were propagated from the experimental uncertainties using the SAMMY code. The uncertainties in brackets, [ ], reflect the external uncertainties as discussed in Section 4.10.8 and presented in Table 4, also in brackets.

The uncertainties in thermal total cross sections given in Table 7 were on the order of ±1σ and were based on the consistency within the data from transmission, capture, multiple sample thicknesses, natural and enriched samples, and various analytical methods.

Table 5
Measured average Γ_γ, referred to as $<\Gamma_\gamma>$, and their uncertainties for europium. The average was measured from the Γ_γ-sensitive resonances and assigned to the insensitive resonances. The uncertainty is the standard deviation of the distribution of Γ_γ values from resonances with $\Gamma_\gamma/\Gamma_n < 5$.

Isotope mass number	Average Γ_γ $<\Gamma_\gamma>$(meV)	Uncertainty in $<\Gamma_\gamma>$(meV)
151	100	10
153	110	20

Table 6
Capture resonance integrals from various nuclear data libraries. Resonance integrals for the europium isotopes are in units of barns. The RPI values were calculated from the measured resonance parameters shown in Table 4 using the NJOY [21] and INTER [22] programs. Uncertainties were propagated from the experimental uncertainties using the SAMMY code. The uncertainties in brackets, [ ], reflect the external uncertainties as discussed in Section 4.10.8 and presented in Table 4, also in brackets. The percent changes of RPI relative to ENDF/B-VII.1[1] are also presented.

	^{151}Eu capture resonance integral (barns)	^{153}Eu capture resonance integral (barns)
RPI	3510 ± 10 [30]	1560 ± 4 [6]
Percent change from ENDF/B-VII.1	+(7 ± 1)%	+(9.9 ± 0.4)%
ENDF/B-VII.1 [1]	3294	1420
ENDF/B-VII.0 [9]	3294	1409
ENDF/B-VI.8 (Rose and Dunford, 1997)	3365	1409
JEFF-3.1 [23]	3356	1409
JENDL-4.0 [24]	3145	1412

Table 7
Thermal cross sections for the europium isotopes in units of barns. The RPI values were calculated from the measured resonance parameters shown in Table 4 using the NJOY[21] and INTER[22] programs. Uncertainties were on the order of ± 1 σ based on the consistency within the data from transmission, capture, multiple sample thicknesses, natural and enriched samples, and various analytical methods. The percent changes of RPI relative to ENDF/B-VII.1[1] are also presented.

	^{151}Eu thermal total cross section (barns)	^{153}Eu thermal total cross section (barns)
RPI	10000 ± 300	340 ± 10
Percent change from ENDF/B-VII.1	+(9 ± 3)%	-(8 ± 3)%
ENDF/B-VII.1 [1]	9187	367
ENDF/B-VII.0 [9]	9187	321
ENDF/B-VI.8 [27]	9176	321
JEFF-3.1 [23]	9170	323
JENDL-4.0 [24]	9170	323

4.10. Components of resonance parameter uncertainties

The components of resonance parameter uncertainty were background, normalization, time zero, resolution function, sample thickness, pulse width, and flight path length. Certain components of uncertainty correspond to the important aspects of the analysis described in the Sections 4.3-4.6. All of the uncertainties were propagated into uncertainties in the resonance parameters using the PUP (Propagated Uncertainty Parameter) feature of SAMMY. The Bayesian SAMMY uncertainties are given in the second, sixth, and tenth columns of Table 4. External uncertainties are given in brackets, [ ], as the third, seventh, and eleventh columns of Table 4 and are described in Section 4.10.8.

4.10.1. Uncertainty in background

For transmission data the uncertainty in the background was propagated from the counting statistics in the notch runs and the quality of the background function fit. Additionally, a shape uncertainty was included based on the agreement of the background function normalized at the fixed notch resonance to a black europium resonance elsewhere in the spectrum. The black resonances

in europium appeared in the thickest samples at 3.38 eV for the epithermal data and 0.46 eV for the thermal data.

For capture measurements two empty sample holders are placed in the sample rotation throughout the experiments to measure background. The difference between the signals from these two empty sample holders was used as an estimate of the uncertainty of the background in the neutron capture measurements; this uncertainty is typically 5%.

4.10.2. Uncertainty in normalization

The normalization for transmission data was set to unity and not fitted in the SAMMY analysis. An uncertainty in the normalization was propagated into the resonance parameters. A fluctuation in beam monitor stability of 1.4% for the thermal measurement and 2% for the epithermal measurement was observed. Each sample was cycled in and out of the beam to reduce the effect of beam monitor fluctuations. However, to be conservative, the uncertainty in transmission normalization was set to 1.4% for thermal data and 2% for epithermal data in the SAMMY analysis.

For the capture measurements the neutron flux was normalized to black europium resonances as described in Section 3.1. An uncertainty of 1% for the thermal measurement and 3.7% for the epithermal measurement was included in the resonance parameter analysis due to beam monitor stability and differences between multiple flux measurements.

4.10.3. Uncertainty in the zero time measurement

The uncertainty of the zero time in the epithermal measurements is less than 1 ns and is based on the counting statistics propagated into a Gaussian fit to the gamma flash data. For the thermal measurements the pulse shape is asymmetric and there are fewer counts leading to uncertainties up to one channel width, 26 ns. But the effect on energy in the thermal region is small.

4.10.4. Uncertainty in the resolution function

The uncertainties in resolution function parameters have been obtained from measurements of uranium in the various measurement configurations (Barry, 2003; Leinweber et al., 2010; Trbovich, 2003) and propagated into all of the resonance parameter uncertainties given in Table 4.

4.10.5. Uncertainty in the sample thickness

Uncertainties based on multiple measurements of sample diameter dominate the small uncertainty in the mass measurement, which used an electronic balance. Thin samples were X-rayed and the uncertainties in their thickness distributions, as documented in Ref. (Geuther et al., 2013), were propagated into the final resonance parameters given in Table 4. No uncertainties in the sample uniformity profiles from Ref. (Geuther et al., 2013) were used.

4.10.6. Uncertainty in the pulse width

Measurements of the gamma pulse produced at the beginning of each LINAC pulse were measured and analyzed to determine the width and uncertainty in the width of the pulse in units of time. Pulse widths are given in Table 1. The electron pulse appears Gaussian for the narrow pulses used in the epithermal measurements. The uncertainties in these pulse widths were less than 1 ns. The wide pulses used in the thermal measurements are irregularly shaped and have a larger uncertainty, up to 20% of pulse width. Experience has shown that these uncertainties do not contribute substantially to resonance parameter uncertainties. All pulse width uncertainties have been propagated into the final resonance parameters.

4.10.7. Uncertainty in the flight path length

Flight path lengths and their uncertainties are given in Table 1. The uncertainties in flight path lengths were based on the alignment of resonance energies in transmission and capture measurements, the alignment of epithermal and thermal measurements, and the consistencies to previous measurements for similar experimental configurations. Part of these uncertainties may be attributed to the moderation thickness of the target. All flight path length uncertainties have been propagated into the final resonance parameters.

4.10.8. External uncertainties from individual sample fits

An external uncertainty is associated with the variability between independent measurements of the same quantity. The present measurements are correlated between and within measurements, but these correlations are not accounted for in this uncertainty analysis. An ensemble of individual sample fits does not take advantage of the Bayesian treatment of a SAMMY multi-sample fit. The external uncertainty is a weighted, by internal uncertainties, standard deviation of the distribution of values from the individual sample fits. The use of external uncertainties from individual sample fits results in larger, more conservative values than the use of exclusively internal uncertainties as provided by SAMMY. External average values and uncertainties were weighted by the internal uncertainty of each component measurement.

Internal uncertainty is the term assigned to conventional propagation of counting statistical uncertainties and the like. SAMMY does not account for the external uncertainties between measurements. The central values for resonance parameters were compared between a multi-sample SAMMY fit and a weighted, by internal uncertainties, average of individual sample fits. The results agreed within internal uncertainties. The internal uncertainty in the average value from individual sample fits was similar to the SAMMY uncertainty from a multi-sample Bayesian fit given in Table 4.

The uncertainty given in brackets, [ ], for each resonance in Table 4 is the external uncertainty between individual sample fits. This value is often larger than the Bayesian or internal estimates of uncertainty. It may be conservative because it does not benefit from the Bayesian treatment of multiple samples.

4.11. Nuclear statistics

4.11.1. Average level spacing

Ten new resonances have been recommended within the previously resolved resonance region for ^{151}Eu below 100 eV. A staircase plot of level density is shown in Fig. 8 for ^{151}Eu and in Fig. 9 for ^{153}Eu. The average level spacing, D_0, is the inverse of the slope of each straight line fit up to the point where D_0 falls below a constant value indicating that levels are being missed in the resonance analysis. The level density for ^{151}Eu shown in Fig. 8 was judged to be constant up to 100 eV with a D_0 of (0.98 ± 0.03) eV as shown in Table 8. The level density for ^{153}Eu shown in Fig. 9 was judged to be constant up to 160 eV with a D_0 of (1.48 ± 0.08) eV as shown in Table 8. Table 8 also provides comparison to the values from Mughabghab (2006).

4.11.2. Neutron width distributions

Cumulative reduced neutron width distributions for the present measurements and ENDF/B-VII.1 are shown in Fig. 10. The figure compares the distributions to those predicted from Porter-Thomas theory (Porter and Thomas, 1956). The new data for ^{151}Eu show some improvement in the number of narrow-width resonances compared to theory. But, there are now more strong resonances than expected. For ^{153}Eu the present measurement confirms the

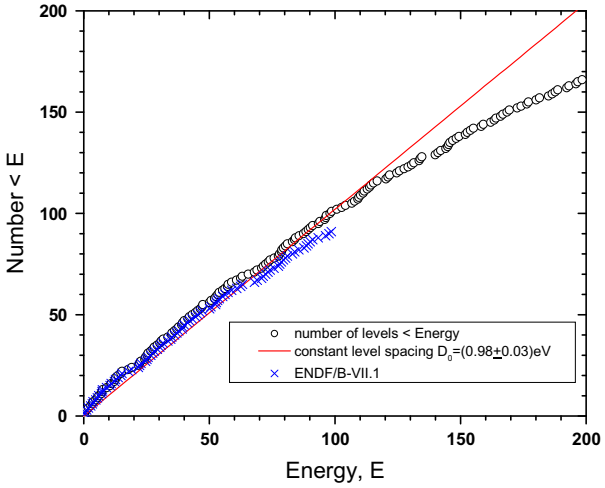

Fig. 8. Staircase plot of level density for ^{151}Eu. The line of constant level density corresponds to an average level spacing, D_0 = 0.98 ± 0.03 eV.

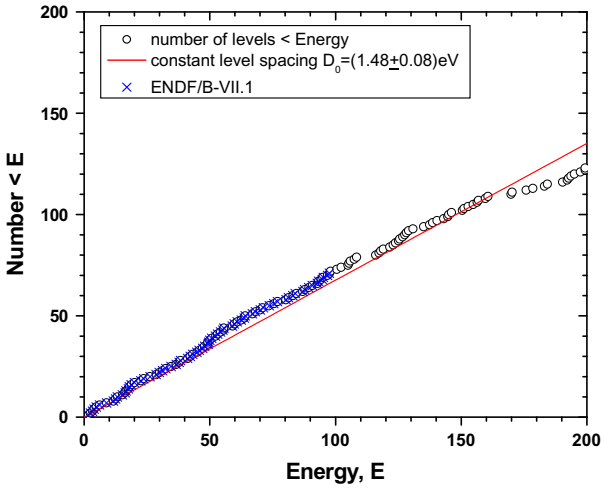

Fig. 9. Staircase plot of level density for ^{153}Eu. The line of constant level density corresponds to an average level spacing, D_0 = 1.48 ± 0.08 eV.

ENDF/B-VII.1 assessment that the number of narrow resonances is smaller than expected.

The data shown in Fig. 10 include all resonances below 100 eV where spin states were assigned. Each data point shown in Fig. 10 was calculated using the average value, $< \Gamma_n^0 >$, specific to each spin group. Then the population of ratios, $\Gamma_n^0 / < \Gamma_n^0 >$, were plotted for each isotope.

Neutron strength functions, S_0, were measured for both naturally-occurring isotopes, ^{151}Eu and ^{153}Eu. The measured values are compared to those of ENDF/B-VII.1 and the Atlas of Neutron Resonances (Mughabghab, 2006) in Table 9. The RPI values were determined from resonances within the energy range where the level density is constant. The s-wave strength for ^{151}Eu is slightly larger than that from ENDF/B-VII.1. The values of S_0 for both isotopes fall within uncertainties of the Atlas and the present measurement.

4.11.3. Radiation width distributions

The neutron transmission and capture measurements revealed radiation width information from too few resonances to present radiation width distributions. Radiation widths were varied according to the criteria discussed in Section 4.8 and the results are shown in Table 4.

Table 8
Statistics on the level density and neutron width distributions of the europium isotopes.

Level densities		
	D_0, eV, RPI	D_0, eV, Atlas[25]
^{151}Eu	0.98 ± 0.03	0.73 ± 0.07
^{153}Eu	1.48 ± 0.08	1.14 ± 0.08
Reduced neutron width distributions, ^{151}Eu, DF = degrees of freedom of a χ^2 distribution based on the variance of the reduced neutron widths. Each reduced width was divided by the average from its own spin state, then the ratios grouped by isotope.		
		DF = 2/var($\Gamma_n^0 / < \Gamma_n^0 >$)
^{151}Eu RPI		2.14
^{151}Eu ENDF/B-VII.1		1.66
Reduced neutron width distributions, ^{153}Eu, see note for ^{151}Eu above.		
		DF = 2/var($\Gamma_n^0 / < \Gamma_n^0 >$)
^{153}Eu RPI		1.31
^{153}Eu ENDF/B-VII.1		1.23

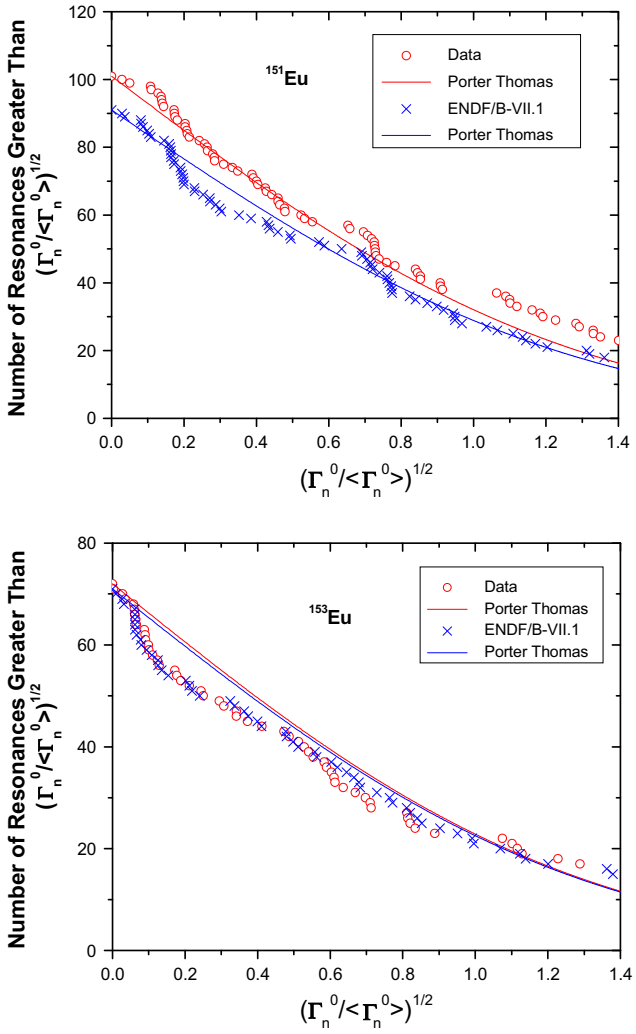

Fig. 10. Cumulative reduced neutron width distributions for the present measurements and ENDF/B-VII.1 compared to Porter Thomas distributions. The new data for ^{151}Eu show some improvement in the number of narrow-width resonances compared to theory. But, there are now more strong resonances than expected. For ^{153}Eu the present measurement confirms the ENDF/B-VII.1 assessment that the number of narrow resonances is smaller than expected.

Table 9
Neutron strength function, S_0, for the naturally-occurring isotopes of Eu.

	S_0 ^{151}Eu ($10^{-4} \times \text{meV}^{-1/2}$)	S_0 ^{153}Eu ($10^{-4} \times \text{meV}^{-1/2}$)
RPI	3.34 ± 0.03	2.4 ± 0.1
ENDF/B-VII.1	3.27	2.32
Atlas of Neutron Resonances	3.1 ± 0.3	2.5 ± 0.2

4.12. Nuclear radii

The nuclear radii used in the final fits of europium data were taken from ENDF/B-VII.1, 8.1 fm for ^{151}Eu, 8.2 fm for ^{153}Eu. The data between resonances in transmission from the ^{153}Eu-enriched samples were analyzed in four regions. The weighted average and uncertainty for the nuclear radius for ^{153}Eu was found to be 8.4 ± 0.4 fm, which is in agreement with the ENDF/B-VII.1 value. There was no region between resonances in the natural Eu data suitable for determining the nuclear radius of ^{151}Eu.

The channel radii that were used for penetrabilities and phase shifts was calculated using Eq. (4) (Larson, 2008).

$$a = 1.23 \times AWRI^{1/3} + 0.8 \quad (4)$$

where a is in fm, and $AWRI$ is the ratio of the atomic weight to the mass of the neutron.

5. Discussion and conclusions

Transmission and capture measurements were performed and analyzed. Experiments tailored separately to the thermal and epithermal energy regions were performed. Natural and ^{153}Eu-enriched samples were measured. Metal non-oxide samples were used exclusively. Resonance parameters were extracted using the Bayesian analysis code SAMMY. The significant features of this measurement and analysis were in the use of enriched and natural samples, the treatment of radiation widths and uncertainties, improved energy resolution, and the extension of the resonance region from 100 eV to 200 eV. This measurement establishes a refinement of the resonance parameters given in ENDF/B-VII.1. One-hundred and twenty-six new resonances have been identified, particularly above 100 eV. The thermal cross sections of ^{151}Eu and ^{153}Eu have been measured to a precision of 3%.

Figs. 3–7 show the quality of the fits to the data. Fig. 3 is an overview of the thermal data. The strong doublet at ≈0.4 eV is prominent in the natural europium data. Fig. 4 shows the intermediate energy region from 10 to 30 eV where thermal and epithermal data sets overlap and all of the data were included in the analysis. In the figure two plots on the left are natural europium, the two on the right are ^{153}Eu-enriched. The top two plots in Fig. 4 are transmission data, the bottom two plots are capture yield. Fig. 5 shows an example of where a new resonance was added in the resolved resonance region. Fig. 6 shows the region above 30 eV where only the high-resolution epithermal data were analyzed. All of the structure above 100 eV was resolved into a recommended set of new resonances whose parameters appear in Table 4. Fig. 7 shows a close-up of a portion of the newly resolved energy region to give the reader an idea of the level of detail and quality of the fits. New resonances were included where the fit was noticeably improved, as in Fig. 5. The staircase plot in Fig. 8 shows that many more levels are needed in the region shown in Fig. 7 for ^{151}Eu. The fits in Fig. 7 could be improved with the addition of those levels.

Great care was taken to encapsulate the highly-reactive metal samples in an inert environment and measure the mass and diameter of the samples before any oxide could form. Extensive X-ray imaging and analysis were performed to quantify any sample nonuniformity (Geuther et al., 2013).

The current estimates of radiation width uncertainties were based upon the conservative method described in Section 4.8. This method addressed the issue of insensitivity of transmission data to radiation widths. Rather than relying on fitted results to data which contained very little radiation width information, a method was employed to determine accurate radiation widths of a few sensitive resonances where measured radiation width information was found in the data. These data-determined average radiation widths were assigned to the insensitive resonances. A distribution of radiation widths was determined for each isotope. The standard deviation of each distribution was used as the uncertainty on the average radiation width, see Table 5.

The determination of transmission background is a crucial task in any resonance parameter analysis. Separate background measurements were made using a suite of notch filters, and a fixed notch was used to provide a definitive background point in the data.

Detailed uncertainty information was compiled for background, capture flux normalization, etc., see Section 4.10. The Propagated Uncertainty Parameter feature of the SAMMY code was used to propagate all known sources of uncertainty into the final result.

Conclusions of the current measurement include an increase of (9 ± 3)% in the thermal total cross section of ^{151}Eu and a (7 ± 1)% increase in the capture resonance integral.

When ENDF/B-VII was updated to release 1 the thermal total cross section of ^{153}Eu was increased by 14% to 367 barns. However, the capture resonance integral was only increased by 1%. Tables 6 and 7 show that the present measurements support an increases of (6 ± 3)% for the thermal total cross section and (10.7 ± 0.4)% for the capture resonance integral of ^{153}Eu over the values from ENDF/B-VII.0. These correspond to a decrease in the thermal total cross section of ^{153}Eu of (8 ± 3)% compared to ENDF/B-VII.1 and an increase in the capture resonance integral of ^{153}Eu of (9.9 ± 0.4)% over ENDF/B-VII.1. The present measurement of thermal total cross section for ^{153}Eu lies between the values from ENDF/B-VII.0 and ENDF/B-VII.1.

References

Anufrijev, V.A. et al., 1979. Resonance parameters of neutron levels for Eu-153, Eu-154 (HL = 8.6 years), Eu-155 (HL = 4.7 years). Atomnaya Energiya 46 (3), 158.

Barry, D.P., 2003. Neodymium Neutron Transmission and Capture Measurements and Development of a New Transmission Detector. PhD thesis Rensselaer Polytechnic Institute.

Block, R.C., Marano, P.J., Drindak, N.J., Feiner, F., Seemann, K.W., Slovacek, R.E., 1988. A multiplicity detector for accurate low-energy neutron capture measurements. In: Proc. Int. Conf. Nuclear Data for Science and Technology, May 30–June 3 1988, Mito, Japan, pp. 383.

Chadwick, M.B. et al., 2006. ENDF/B-VII.0: next generation evaluated nuclear data library for science and technology. Nucl. Data Sheets 107 (12), 2931.

Chadwick, M.B. et al., 2011. ENDF/B-VII.1: nuclear data for science and technology: cross sections, covariances, fission product yields and decay data. Nucl. Data Sheets 112, 2887.

Danon, Y., Block, R.C., 2002. Minimizing the statistical error of resonance parameters and cross sections derived from transmission measurements. Nucl. Instrum. Meth. Phys. Res. A 485, 585.

Danon, Y., Slovacek, R.E., Block, R.C., 1993. The enhanced thermal neutron target at the RPI LINAC. Trans. Am. Nucl. Soc. 68, 473.

Danon, Y., Slovacek, R.E., Block, R.C., 1995. Design and construction of a thermal neutron target for the RPI LINAC. Nucl. Instrum. Meth. Phys. Res. A 352, 596.

Dunford, C.L., 2001. ENDF Utility Codes Release 6.12, Informal Report.

Geuther, J.A., Block, R.C., Methe, B., Barry, D.P., Leinweber, G., 2013. X-ray determination of the thickness of thin metal foils. accepted for publication in Journal of X-Ray Science and Technology.

Konks, V.A., Popov, Y.P., Fenin, Y.I., 1968. Radiative capture of neutrons by nuclei with A = 140–200. Sov. J. Nucl. Phys. 7, 310.

Larson, N.M., 2008. Updated Users' Guide for SAMMY: Multilevel R-Matrix Fits to Neutron Data Using Bayes' Equations", ORNL/TM-9179/R8 ENDF-364/R2, Oak Ridge National Laboratory (October 2008).

Lee, J.H., Hori, J., Nakajima, K., 2010. Measurement of ^{151,153}Eu neutron capture cross sections using a pair of C6D6 detectors. In: Proceedings of the 2010 Symposium on Nuclear Data, November 25–26, 2010, Kasuga, Japan, pp. 101.

Leinweber, G., Burke, J.A., Knox, H.D., Drindak, N.J., Mesh, D.W., Haines, W.T., Ballad, R.V., Block, R.C., Slovacek, R.E., Werner, C.J., Trbovich, M.J., Barry, D.P., Sato, T., 2002. Neutron capture and transmission measurements and resonance parameter analysis of samarium. Nucl. Sci. Eng. 142, 1.

Leinweber, G., Barry, D.P., Burke, J.A., Drindak, N.J., Danon, Y., Block, R.C., Francis, N.C., Moretti, B.E., 2010. Resonance parameters and uncertainties derived from epithermal neutron capture and transmission measurements of natural molybdenum. Nucl. Sci. Eng. 164, 287.

MacFARLANE, R.E., Muir, D.W., 1994. The NJOY Nuclear Data Processing System Version 91", LA-12740-M, Los Alamos National Laboratory.

Moxon, M.C., Endacott, D.A.J., Jolly, J.E., 1976. The neutron capture cross-section of ^{151}Eu and ^{153}Eu in the energy range 0.1–100 keV. Ann. Nucl. Energy 3, 399.

Mughabghab, S.F., 2006. Atlas of Neutron Resonances, fifth ed. Elsevier, New York.

Overberg, M.E., Moretti, B.E., Slovacek, R.E., Block, R.C., 1999. Photoneutron target development for the RPI linear accelerator. Nucl. Instrum. Meth. Phys. Res. A 438, 253.

Parker, W.E. et al., 2007. Review of livermore-led neutron capture studies using DANCE. In: Proceedings of International Conference on Nuclear Data for Science and Technology, April 22–27, 2007, Nice, France. pp. 491.

Porter, C.E., Thomas, R.G., 1956. Fluctuations of nuclear reaction widths. Phys. Rev. 104, 483.

Rahn, F. et al., 1972. Neutron resonance spectroscopy. IX. The separated isotopes of samarium and europium. Phys. Rev. C 6 (1), 251.

Rose, P.F., Dunford, C.L., 1997. ENDF-102 Data Formats and Procedures for the Evaluated Nuclear Data File ENDF-6", BNL-NCS-44945, Rev. 2, Brookhaven National Laboratory.

Santamarina, A. et al., 2009. Validation results from JEF-2.2 to JEFF-3.1.1, Nuclear Energy Agency Data Bank, OECD, JEFF Report 22, NEA No. 6807.

Shibata, K. et al., 2011. JENDL-4.0: a new library for nuclear science and engineering. J. Nucl. Sci. Technol. 48, 1.

Trbovich, M.J., 2003. Hafnium Neutron Cross Sections and Resonance Analysis. PhD thesis, Rensselaer Polytechnic Institute.

Widder, F., 1974. Neutron capture cross section measurements in the energy region from 0.01 to 10 electron volts. In: Proceedings of the 2nd International Symposium on Neutron Capture Gamma-Ray Spectroscopy, Petten, pp. 265.